MASTERARBEIT | MASTER'S THESIS

Titel | Title

Effects of VEGF-C-presenting MSC-derived extracellular vesicles on lymphatic endothelial cells

verfasst von | submitted by

Alireza Sahl Abadi BSc

angestrebter akademischer Grad | in partial fulfilment of the requirements for the degree of

Master of Science (MSc)

Wien | Vienna, 2025

Studienkennzahl lt. Studienblatt | Degree programme code as it appears on the student record sheet:	UA 066 865
Studienrichtung lt. Studienblatt | Degree programme as it appears on the student record sheet:	Masterstudium Molecular Biology
Betreut von | Supervisor:	Assoc. Prof. Dr. Johannes Grillari

Table of Contents

Acknowledgments

I would like to sincerely thank Professor Johannes Grillari and Priv.-Doz. Mag. Dr. Wolfgang Holnthoner for their valuable feedback and for giving me the opportunity to carry out my master's thesis at the LBI. I am especially grateful to my co-supervisor, Johannes Oesterreicher, for his patient guidance, encouragement, and continuous support throughout this project, through which I have learned a great deal, and which has been invaluable for my development as a scientist during this thesis. My heartfelt thanks also go to Phillip Sabler and the entire EXBT group at the LBI for their support, assistance, and the many ways they made my work and time at the institute enjoyable and rewarding.

Abstract

Lymphedema, a chronic condition caused by impaired and insufficient lymphatic fluid drainage resulting in its subsequent accumulation, may be alleviated by promoting lymphangiogenesis through stimulation of lymphatic endothelial cells (LECs). Extracellular vesicles (EVs) are increasingly viewed as important mediators of intercellular communication with strong potential in regenerative medicine due to their ability to carry bioactive molecules, high biocompatibility, and capacity to cross biological barriers. Targeting LECs with EVs to enhance lymphangiogenesis offers a promising therapeutic strategy for restoring interstitial fluid balance in affected tissues. For this purpose, engineered EVs expressing recombinant CD81-P1-VEGF-C constructs to target vascular endothelial growth factor receptor 3 (VEGFR-3) on the target cells were put to the test to examine potential improvements in cell binding, uptake, proliferation, and migration compared to wild-type (WT). To assess the binding and uptake of engineered EVs to target VEGFR3 receptors on target cells, namely, human dermal LECs (HDLECs) and engineered BaF3 cells, the EVs were stained with CellMask™ Deep Red (CMDR), a highly effective lipophilic membrane dye, and their interaction with cells was subsequently examined by flow cytometry. Other techniques, such as dot blot, scratch assay, alamarBlue, and MTT assays, were also utilized to characterize and assess EV function, receptor activation, and induction of cell proliferation and migration. The results show a promising advantage of the recombinant constructs in all the aforementioned parameters compared to WT, showcasing exciting potential for future research.

Zussamenfassung

Lymphödem, eine chronische Erkrankung, die durch beeinträchtigten und unzureichenden Abfluss von Lymphflüssigkeit und deren anschließende Ansammlung verursacht wird, kann möglicherweise durch die Förderung der Lymphangiogenese mittels Stimulation von lymphatischen Endothelzellen (LECs) gelindert werden. Extrazelluläre Vesikel (EVs) werden zunehmend als wichtige Mediatoren der interzellulären Kommunikation betrachtet, mit starkem Potenzial in der regenerativen Medizin aufgrund ihrer Fähigkeit, bioaktive Moleküle zu transportieren, ihrer hohen Biokompatibilität und ihrer Kapazität, biologische Barrieren zu überwinden. Das gezielte Ansprechen von LECs mit EVs zur Verstärkung der Lymphangiogenese bietet eine vielversprechende therapeutische Strategie zur Wiederherstellung des interstitiellen Flüssigkeitsgleichgewichts in betroffenen Geweben. Zu diesem Zweck wurden gentechnisch veränderte EVs, die rekombinante CD81-P1-VEGF-C-Konstrukte exprimieren und den vaskulären endothelialen Wachstumsfaktor-Rezeptor 3 (VEGFR-3) auf den Zielzellen adressieren, getestet, um mögliche Verbesserungen in Zellbindung, Aufnahme, Proliferation und Migration im Vergleich zum WT zu untersuchen. Um die Bindung und Aufnahme der modifizierten EVs an die Ziel-VEGFR3-Rezeptoren auf Zielzellen, nämlich humane dermale LECs (HDLECs) und gentechnisch veränderte BaF3-Zellen, zu evaluieren, wurden die EVs mit CellMask™ Deep Red (CMDR), einem hochwirksamen lipophilen Membranfärbemittel, markiert und ihre Interaktion mit Zellen anschließend mittels Durchflusszytometrie analysiert. Weitere Techniken, wie Dot Blot, Scratch Assay, alamarBlue- und MTT-Assays, wurden ebenfalls eingesetzt, um die Funktion der EVs, die Rezeptoraktivierung sowie die Induktion von Zellproliferation und -migration zu charakterisieren und zu bewerten. Die Ergebnisse zeigen einen deutlichen Vorteil der rekombinanten Konstrukte in allen genannten Parametern im Vergleich zum WT und verdeutlichen ein spannendes Potenzial für zukünftige Forschung.

1. Introduction

1.1. Human vasculature system

The human vascular system consists of two distinct networks: blood vessels and lymphatic vessels. Each system possesses unique anatomical structures and functions, with endothelial cells (ECs) exhibiting specific phenotypic and molecular characteristics [1]. The primary role of the blood vasculature, which is lined by an inner lining of blood vascular endothelial cells (BECs), is to distribute blood and its components throughout the body, whereas the lymphatic system, composed of a single layer of lymphatic endothelial cells (LECs), is responsible for the continuous removal of interstitial fluid and the facilitation of immune cell transport and interaction [2], [3], [4]. Despite being separate, these vessels are closely situated within various tissues, forming highly interconnected regions known as the microvasculature, Fig. 1, in which significant fluid and molecular exchange occurs between the two systems [5]. Here, roughly 90% of the fluid filtered by blood capillaries is reabsorbed at the venous end, while the remaining 10% becomes lymph, which is drained by lymphatic capillaries to return the excess fluid back to the bloodstream [6].

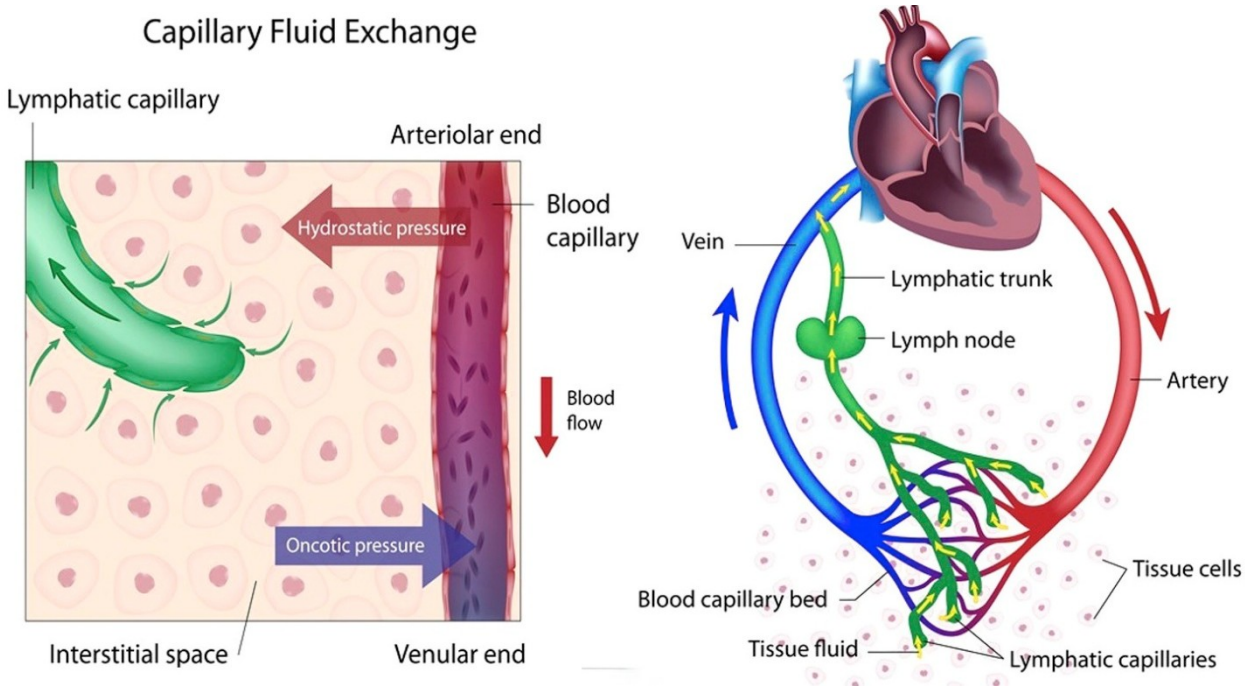

Figure 1 An illustration of tissue fluid drainage via lymph capillaries from the interstitial space and the lymphatic circulation returning the lymph to the bloodstream. *[6]*

1.1.1. Lymphatic vs blood endothelial cells

LECs are specialized endothelial cells that line the lymphatic vasculature, which play a key role in maintaining interstitial fluid homeostasis, immune surveillance, and the transport of macromolecules [7],[4]. They are distinct from blood endothelial cells (BECs) by their expression of specific molecular markers, including LYVE-1, Prox-1, podoplanin, and VEGFR-3, while both cell types share pan-endothelial markers such as CD31 [8], [9]. Morphologically, LECs are characterized by overlapping, discontinuous intercellular junctions and an abundance of cytoplasmic vesicles, adaptations that facilitate their specialized roles in fluid and protein uptake [10].

1.1.2. Lymphedema

Lymphedema is a chronic condition characterized by the abnormal buildup of lymphatic fluid, leading to inflammation and swelling that may cause long-term changes in the skin and underlying tissues. This occurs when the accumulation of protein-rich fluid within the fibro-adipose tissue and the interstitium and surpasses the capability of the lymphatic system to drain and transport the lymphatic fluid [11]. There are two types of Lymphedema, namely, primary and secondary lymphedema. Primary lymphoedema (PLE) occurs as a result of defects in the development or function of the lymphatic system. It can emerge as part of a syndrome or in an isolated non-syndromic manner and may be present at birth or have an onset later in life. Mutations have been identified in several genes involved in the early formation of lymphatic vessels and valves, as well as in the growth and expansion of the lymphatic system and its pathways, in both syndromic and non-syndromic forms of PLE. Consequently, the current hypothesis is that most cases of PLE have a genetic origin, although a causative mutation is detected in only about one-third of affected individuals. Secondary Lymphedema (SLE), which is the most frequent subtype of lymphoedema, however, occurs because of damage to the healthy lymphatics caused by factors such as infections, invasive injury, or morbid obesity; hence, SLE, in contrast to PLE, is the acquired subtype of lymphedema [12][6].

A potential solution to alleviate this issue would be to enhance the capability of the lymphvascular system to clear the excessive buildup of interstitial fluid by expanding its network throughout the tissues. Achieving this requires the promotion of

lymphangiogenesis, the extension of lymphatic vessels sprouting from pre-existing vessels driven by LECs [13], especially within the affected regions.

1.1.3. VEGF family

The vascular endothelial growth factor (VEGF) is a group of cytokines that play a key role in vasculogenesis, angiogenesis, and lymphangiogenesis. In mammals, the VEGF protein family consists of VEGF-A, VEGF-B, VEGF-C, VEGF-D, and placental growth factor (PlGF) [14] . VEGF-A is the founding and most studied member, possessing a range of functions, such as pro-angiogenic activity, increasing vascular permeability, and the stimulation of cell migration in endothelial cells and the macrophage lineage.[15] VEGF-A, alongside VEGF-B and PlGF, comprises isoforms, resulting from their alternative exon splicing [16]. Compared to other VEGF homologs, VEGF-B does not play a major role in angiogenesis but is rather critical for blood vessel survival under pathological conditions. This survival effect is not only on vascular EC but also on vascular smooth muscle cells and pericytes [17]. A recent study has demonstrated that the VEGF-B isoform, VEGF-B186, is a novel mediator of endoplasmic reticulum (ER) stress and can induce cardiac regeneration by stimulating the unfolded protein response (UPR) through RGD-binding integrins and ER stress pathways, independent of VEGFR-1 and neuropilin [18]. VEGF-C and VEGF-D (also known as c-Fos-induced growth factor, FIGF) are both structurally and functionally related [19], and are synthesized as inactive precursors that require proteolytic processing by protein convertases [20]. VEGF-C and VEGF-D regulate lymphangiogenesis via VEGFR-3 and facilitate angiogenesis through VEGFR-2 under specific conditions [21]. VEGF-D is distinct from VEGF-C in expression patterns, mainly found in the lungs, heart, skeletal muscle, and intestines [22]. PlGF is primarily expressed in the placenta and promotes the development and maturation of the placental vascular system. In adults, PlGF is also expressed at low levels in many other tissues, such as the lung, heart, thyroid and liver, where it plays an important role in angiogenesis in response to pathological ischemia or injury. PlGF promotes angiogenesis by competitively binding to the VEGFR-1 receptor, resulting in an enhanced VEGF-A/VEGFR-2 binding, which has stronger tyrosine kinase activity [23].

There are three main types of VEGF receptors (VEGFR) related to VEGFs signaling: namely, VEGFR-1 (also known as Flt-1), VEGFR-2 (also referred to as KDR in humans and Flk-1 in mice), and VEGFR-3 (also known as Flt-4), predominantly expressed in endothelial cells [24]. VEGFRs are formed by two monomers with several extracellular immunoglobulin domains each, which mediate ligand binding. The monomers also contain a transmembrane chain and an intracellular effector comprising two regions with tyrosine kinase activity [25]. VEGF-A binds VEGFR-1 and VEGFR-2, VEGF-B and PlGF can bind to VEGFR-1, and VEGF-C and VEGF-D are able to bind to VEGFR-3 and to VEGFR-2 after proteolytic cleavage [26], [27]. Furthermore, another class of receptors: neuropilins (NRPs), initially considered as independent receptors for class 3 semaphorins, a family of soluble molecules with neuronal guidance functions, are now also recognized as co-receptors for the VEGFRs [28], and a wide range of transmembrane receptors. As shown in Fig. 2, while all five aforementioned VEGF homologs bind both Neuropillin-1 and 2, VEGF-B only binds Neuropillin-1 [29].

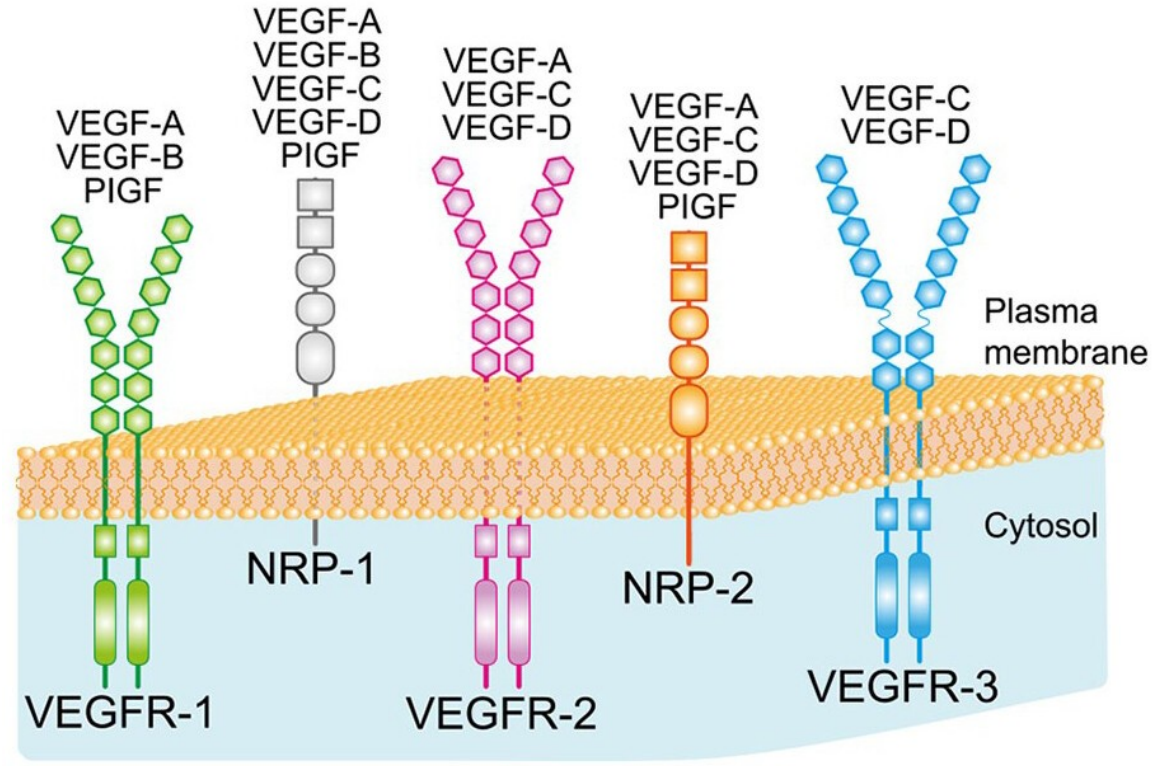

***Figure 2 An illustration of VEGF proteins and their receptors**. [29]*

1.1.4. VEGF-C

VEGF-C and its primary receptor, VEGFR-3, are central components in the regulation of lymphangiogenesis [30]. VEGF-C is synthesized as a pro-peptide, and to generate its mature and bioactive form, a proteolytic cleavage of its C-terminal by specific proteases is necessary. This processing event critically changes both the pathological and physiological bioactivity of VEGF-C [31], [32]. The VEGF-C variant used in this experiment had previously been cleaved by a serine protease, Plasmin [33], for the subsequent activation to its bioactive form, hence named as P1-VEGF-C. This variant was then sequenced and the respective genes stably integrated via transduction into immortalized adipose-derived stromal cells (ASCs) hTERT 300, from which the Extracellular vesicles (EVs) were isolated, Fig. 3.

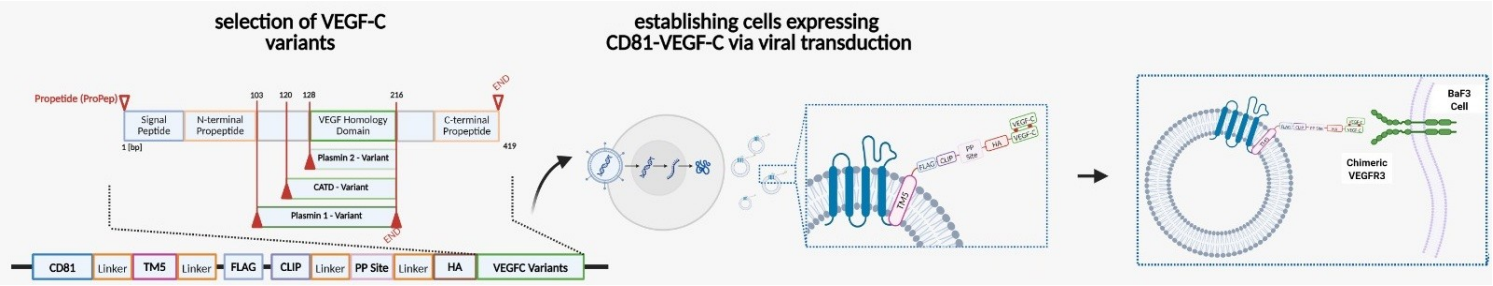

Figure 3 An illustration of the VEGF-C variant processing and its subsequent CD81-bound construct interacting with a chimeric VEGFR3 on engineered BaF3 cells. *© Johannes Oesterreicher*

VEGF-C primarily binds VEGFR-3, Fig. 4, and to a lesser extent, VEGFR-2. Through these receptor interactions, VEGF-C promotes the proliferation, survival and migration of LECs, making it essential for the formation and maintenance of the lymphatic system.[10] Under certain conditions, VEGF-C can also promote angiogenesis by activating VEGFR-2 [30]. Upon ligand binding, VEGFR-3 forms either homodimers or heterodimers with VEGFR-2, initiating downstream signaling cascades such as the AKT and ERK pathways, which are essential for endothelial cell survival

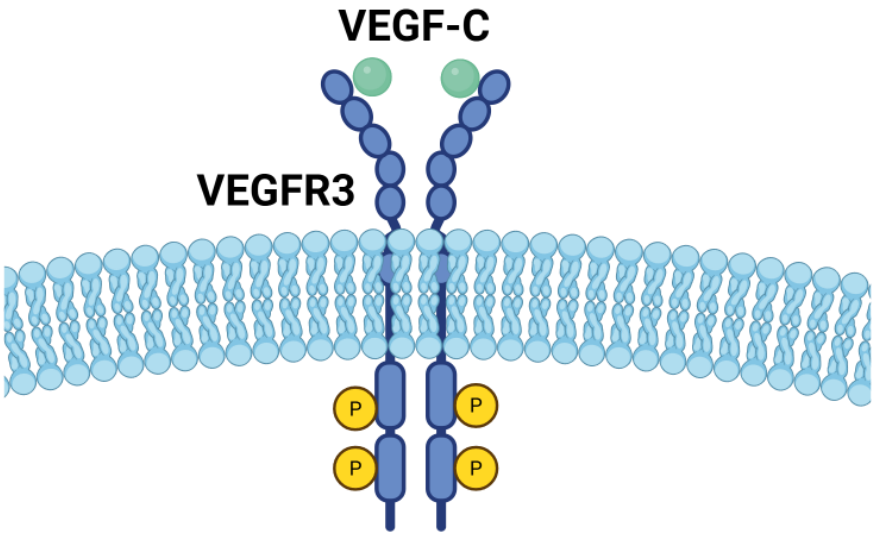

Figure 4 An illustration of the VEGF-C/VEGFR3 binding and dimerization.

and migration [34]. VEGFR-2/VEGFR-3 heterodimer formation favorably promotes phosphoinositide 3-kinase (PI3K)–dependent activation of protein kinase B (AKT), whereas VEGFR-3 homodimers primarily stimulate p42/p44 mitogen–activated protein kinase (MAPK, also known as ERK1/2) activation [35], [36]. Effectors acting downstream of ERK, namely cAMP response element (CRE)–binding protein (CREB) and nuclear transcription factors Ets-1/2, promote cell proliferation, differentiation, and angiogenesis by upregulating, among others, the expression of MMPs (Matrix Metalloproteinases) and growth factors such as VEGFs. Downstream AKT effectors, mTOR (mechanistic target of rapamycin) complex (mTORC1), and endothelial nitric oxide synthase (eNOS) mainly enhance cell survival and growth functions by promoting the expression of transcription factors such as MAFB, KLF4, and SOX18 in the LECs. Interaction between the AKT and ERK signaling pathways enables context-dependent and precise regulation of lymphatic endothelial cell functions [37], [38], [39]. It is also worth mentioning that this signaling axis also plays a role in pathological settings such as cancer metastasis and chronic inflammation, where excess lymphangiogenesis can contribute to disease progression [40]. To study the interaction between VEGF-C and VEGFR-3, a variant of BaF3 cells, Fig. 3, an immortalized murine pro-B cell line was utilized, which was previously engineered to overexpress chimeric receptors composed of a VEGFR-3 extracellular domain and an EpoR intracellular domain. This enables these otherwise IL-3 dependent cells to also be able to survive and proliferate via VEGF-C supplementation. [41]

Therapeutic delivery of VEGF-C and its targeted delivery can be carried out through various methods, including direct local or systemic injection of the recombinant protein, gene transfer using viral vectors, mRNA packaged in lipid nanoparticles, antibody-guided targeting, or through EVs. While each method offers unique advantages, they also present limitations and challenges, such as immune responses or immunogenicity risks, especially with viral vectors and some mRNA lipid nanoparticles, the short half-life of recombinant proteins requiring frequent dosing with recombinant protein injection, limited control over expression duration with viral vectors, potential off-target toxicities in systemic injections, and difficulties in tissue-specific targeting or penetration [42], [43], [44], [45]. Therefore, EVs were selected and utilized in this study due to their low immunogenicity, and the ability to cross biological barriers, making them an ideal candidate for drug delivery and regenerative medicine [46].

1.2. Extracellular vesicles

EVs have emerged as promising therapeutic tools with the potential to play a key role in the future of medicine. Previously viewed as simple cellular byproducts, they are now recognized as key mediators of intercellular communication, transporting bioactive molecules such as proteins, nucleic acids and lipids with high specificity [47].

1.2.1. Biogenesis

EVs are membrane-bound nanoparticles essential for intercellular communication, released by all cell types. These bilipid nanoparticles come in three main subtypes: exosomes, microvesicles, and apoptotic bodies, which are categorized according to their biogenesis, size, release mechanisms, function, and content [48]. Apoptotic bodies are released during cell apoptosis through the separation of the plasma membrane from the cytoskeleton, often ranging from 1-5 μm in diameter. Microvesicles bud off directly from the plasma membrane, varying from 0.1 - 1 μm in diameter, and exosomes are formed by an endosomal pathway, derived from multivesicular bodies, and range from 30-150 nm in diameter [49]. EVs carry cell-specific cargo, including proteins, lipids, metabolites, and nucleic acids, and play roles in immune responses, tissue repair, and cancer progression. Their varied physical properties, such as size and membrane composition, allow for the enrichment of specific subtypes [50]. EVs primarily travel through blood and lymph, facilitating paracrine communication [51]. While blood-

derived EVs are well-studied, more research should be carried out on those originating from LECs. Understanding EVs' diverse nature and functions offers insights into their potential as disease biomarkers and therapeutic vehicles.

1.2.2. Uptake

EV uptake by cells involves the internalization of these membrane-bound particles via various endocytic pathways, including clathrin-dependent, caveolin-mediated, or lipid raft-mediated endocytosis, phagocytosis, macropinocytosis, and direct fusion [52] [53]. The specific pathway depends on surface molecules present on both the EV and the recipient cell. Although the process is usually fast and energy-dependent, it is relatively inefficient, as only about 1% of EVs are internalized per hour, and around 30% of those manage to deliver their cargo into the cytosol [54]. Despite this low efficiency, EV uptake is a tightly regulated and biologically significant mechanism for cell-to-cell communication.

1.2.3. EV engineering

An important factor that makes EVs potent therapeutic tools and overcomes their limitations is the possibility to bioengineer their composition, cargo, or surface of EVs through genetic, chemical, or physical approaches, to enhance cargo loading, targeting, and drug delivery. Genetic fusion of therapeutic proteins to EV-sorting domains like tetraspanins enables endogenous incorporation during vesicle biogenesis, whereas physical methods such as electroporation and sonication allow post-isolation cargo loading [55]. Surface modifications include presenting targeting ligands via chemical conjugation or genetic engineering and incorporating fusogenic proteins like VSV-G to improve endosomal escape and cytosolic delivery. Furthermore, pH-sensitive inteins can also be utilized for controlled cargo release and foldon domains to enhance fusion protein stability, creating modular systems capable of delivering proteins, RNA, and genome-editing complexes with high efficiency [56], [57], [58].

1.2.3.1. Snorkel tag

Multipass membrane proteins present unique challenges for inserting a tag as the extracellular regions contain small loops ,ergo introducing an epitope tag risks interfering with the function, structure, or location of the membrane protein [59]. The Engineered EVs utilized in this study were equipped with a snorkel tag, a novel tagging system where an additional transmembrane domain followed by a modifiable tag/protein construct is attached to the cytoplasmic C-terminus of the membrane protein. Hence, the tag is displayed extracellularly and is structurally separate from the membrane protein [59]. This system enables the affinity purification of EVs from complex matrices in a non-destructive form while preserving EV characteristics in terms of surface protein profiles, associated miRNA patterns, and uptake into model cell lines [60]. The snorkel tag has previously been fused to CD81, a member of the tetraspanin family characterized by four transmembrane domains, which is an essential component in the function of extracellular vesicles, particularly exosomes. It plays a vital role in various cellular processes, including cell activation, development, motility and growth [61]. In this project, engineered variants of CD81, namely, CD81-P1-VEGF-C and CD81-P1-VEGF-C/P1-VEGF-C named as recombinant VEGF-C single construct (Single) and recombinant VEGF-C double construct (Double), respectively, were used, each containing a P1-VEGF-C presenting snorkel tag, Fig. 5. In the case of the double construct, the cells were transduced to additionally overexpress soluble P1-VEGF-C proteins to facilitate VEGFR-3 dimerization and activation by increasing its availability and so compare with the single construct.

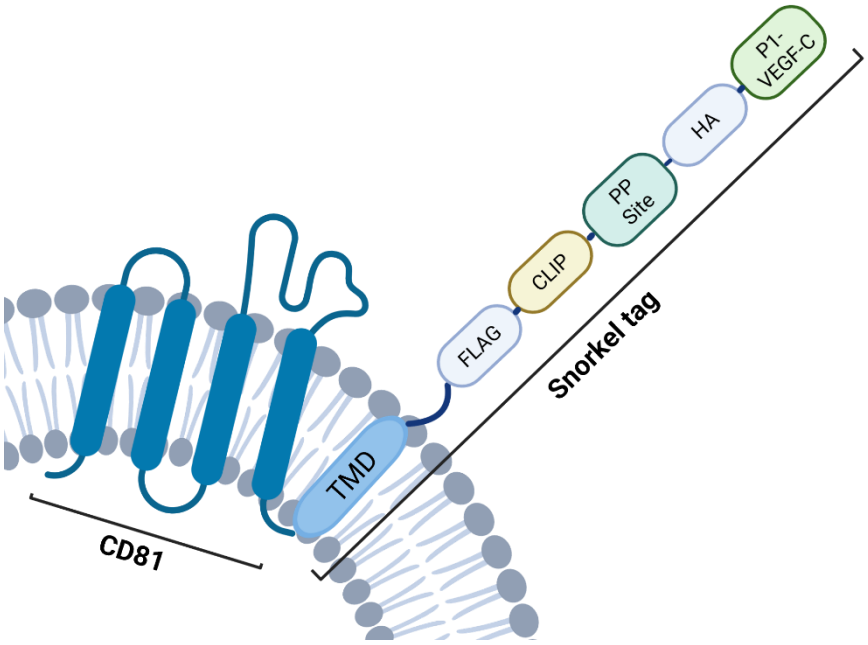

Figure 5 An illustration of the engineered CD81 fused with the VEGF-C presenting snorkel tag.

1.2.4. EV enrichment

To bulk produce engineered EVs, appropriate producer cell lines must first be stably transduced and cultured. For this purpose, Immortalized and well-characterized cells such as ASC hTERT 300, are generally preferred over primary cells, which exhibit limited proliferation capacity, donor variability, and rapid senescence, making them unsuitable for large-scale production [62]. The ASC hTERT 300 have been stably transduced to overexpress human telomerase reverse transcriptase (hTERT), which maintains telomere length, allowing extended proliferation capacity without altering cell karyotype, and so remedies the issue with replicative senescence, which arises when extensively passaging primary cells such as human dermal lymphatic endothelial cells (HDLECs) [63]. Furthermore, research has shown that mesenchymal stem cell-derived EVs (MSC-EVs) cause low immunogenicity and possess immunomodulatory, anti-inflammatory properties [64], making them an ideal candidate for research and cell-based therapies. Given that EV populations are inherently heterogeneous in size, surface markers, and cargo composition, enrichment is an essential step to concentrate the desired EVs, remove unincorporated cargo and debris, and standardize their properties for consistent dosing and purity. For this goal, several

enrichment approaches are available, each with distinct advantages and limitations. Differential ultracentrifugation and density gradient separation are widely used for their ability to yield high-purity EVs but are constrained by low throughput, long run times, and potential vesicle damage. Size-exclusion chromatography offers gentle separation and reproducibility but provides modest resolution and can dilute samples. Tangential flow filtration (TFF) enables scalable, rapid concentration under minimal shear stress, though careful membrane selection is required to avoid clogging. Affinity capture with antibodies or ligands provides high specificity but is costly and may be biased toward certain subpopulations. Polymer-based precipitation is simple and high-yielding but often co-isolates protein contaminants. Finally, emerging microfluidic and acoustic trapping technologies provide precise, low-volume isolation, though scalability is currently limited by throughput and equipment requirements. Overall, these enrichment strategies allow the preparation of uniform, high-purity EVs, improving reproducibility, reducing off-target effects and immune activation, and ensuring safety and efficacy in downstream in vitro and in vivo applications [65], [66], [67].

2. Aim

The goal of this study was to evaluate the potential enhancements that these engineered EVs may offer compared to the WT EVs, and to assess their ability to initiate VEGF-C–dependent pro-lymphendothelial signaling through activation of VEGFR-3. Methods such as Flow cytometry, a powerful technique used in biology and medicine to analyze the physical and chemical characteristics of cells or particles as they flow in a fluid stream through a beam of light [68], vitality assays such as alamarBlue and MTT, in addition to scratch assay, were employed to examine the homing, receptor activation, cell proliferation, and migration effects of the EVs on LECs. This research can provide the groundwork for the future use of targeted EV therapy to enhance lymphangiogenesis, leading to innovative and promising therapeutic methods for treating lymphedema.

3. Materials and Methods

3.1. Materials

3.1.1. Cell lines

The following cell lines were used, namely: BaF3 (LBI for traumatology), HDLEC (Promocell) passages 7-9, and ASC hTERT 300 (Evercyte).

3.1.2. Materials and instruments

Name	Model/Supplier
Flow cytometer	Cytoflex
Microscope	Zeiss
Centrifuge	Hettich
Vortex	Scientific Industries
Incubator	Thermo Scientific
ZetaView Quatt NTA	Particle Metrix
Plate reader	POLARstar Omega
Lamina	Thermo Scientific
MW centrifugal filters (10 K)	Amicon Ultra
Cellometer	Nexcelom
Water bath	Thermo Scientific
Chemidoc™ Imager	Bio Rad
Thermomixer	Eppendorf
Culture-Insert 4 Well in µ-Dish 35 mm	Ibidi

3.1.3. Media, buffer, and solutions

Name	Remarks	Supplier
ddH_2O	-	Fresenius
Antibiotics	Penicillin and Streptomycin (Pen/Strep)	Sigma
Opti-MEM	MEM-RXA Lot No: CP21-4108 w/o L-Glutamine with Nucleosides sterile-filtered	Gibco
MesenCult ACF plus medium	Supplemented with 1% x100 GlutaMAX, 0.2% G418 antibiotics and animal component-free supplement.	STEMCELL TECHNOLOGIES
GlutaMAX	-	Thermo Fischer
DMEM – HG (Dulbecco´s Modified Eagle´s Medium-high glucose)	Supplemented with 10%FCS, 1% Pen/Strep and 50 mM L-Glutamine	SIGMA Life Science
EGM-2	Containing: EBM-2 medium, FCS, hFGF, VEGF, R3-IGF-1, Ascorbic acid, hEGF, GA-1000, Heparin	Lonza
DPBS (Dulbecco's Phosphate Buffered Saline)	-	Sigma
Trypsin EDTA X10	-	Sigma
BSA (Bovine Serum Albumin)	1% and 5% dissolved in DPBS	Sigma
TBST	100 mM Tris Cl Ph 7.4 1500 mM NaCl 10 mM EDTA	-

(Tris-buffered saline with Tween 20)	Diluted to 1x by the addition of 880 ml ultra-pure water. 0.1% Tween	
Trypan blue	-	Gibco
rhVEGF-C	-	STEMCELL TECHNOLOGIES
IL-3 (Interleukin-3)	-	STEMCELL TECHNOLOGIES
CellMask™ Deep Red (CMDR)	Diluted 1:20 in DMSO	Thermo Fischer
Cryostor™	-	Sigma
FCS (Fetal Calf Serum)	-	Thermo Fisher
TrypLE™ Select	-	Thermo Fischer
animal component-free coating substrate	Diluted 1:300 in DPBS	STEMCELL TECHNOLOGIES
AlamarBlue ™ HS Cell viability Reagent	invitrogen	Thermo Scientific
Clarity ™ Western ECL Substrate	Luminol/enhancer solution Peroxide solution	BIO-RAD
Antibodies: **Primary** **Secondary**	all diluted 1:1000 in 1% BSA-TBST: CD81 (mouse) TSG101(rat) Syntenin-1 (mouse) Calnexin (rabbit) All HRP conjugated: Anti-mouse Anti-rat Anti-rabbit	 ThermoFischer(#11525542) Abcam(#ab125011) Origene(#TA504796) Abcam(#22595) Abcam (#205719) Invitrogen (#ZD392001) Antibodies-online inc. (#ABIN101990)

3.2. Methods

3.2.1. Cell thawing and seeding

Consistent for all utilized cell types, the cells were thawed, mixed in 10 ml warm medium, and centrifuged for 5 minutes at 300 x g. Next, the cells were resuspended in the respective media and transferred to a flask, and incubated at 37°C.

3.2.2. Standard cell cultivation of the ASC hTERT 300 cells

Prior to seeding, the flasks were coated with animal component-free coating substrate diluted 1:300 in Dulbecco's Phosphate Buffered Saline (DPBS) (8 ml for T75 flasks) and either left in the fridge overnight or for 3 hours at room temperature. The cells were then seeded in MesenCult™ - ACF plus medium.

3.2.3. Standard cell cultivation of the BaF3 cells

The cells were cultured in DMEM-HG medium supplemented with 5 ng/ml m-IL3 or 25 ng/ml rhVEGF-C to stimulate growth, and incubated at 37°C. The cells were grown to ~ 90-100% confluence before analysis.

3.2.4. Standard cell cultivation of the HDLECs

The cells, passages 7-9, were cultured in EGM-2 medium supplemented with 50 ng/ml rhVEGF-C to stimulate growth, and incubated at 37°C. The cells were grown to ~ 80% confluence before analysis.

3.2.5. Cell handling

Consistent for all utilized cell types, the medium was initially removed, and the cells were washed twice with 10 ml of PBS. Next, 2 ml of TrypLE™ Select (1X) were added to the flask, incubated for 3 mins at 37°C, collected by washing twice with 10 ml OptiMEM medium, centrifuged, and resuspended in the respective medium. To count,

the cells were harvested, the suspension was mixed with a ratio of 1:1 or 1:10 with Trypanblue solution and applied to a Hemocytometer to be observed under a microscope manually or with a Nexcelom Celometer®. To freeze the cells, the BaF3 cells were harvested, centrifuged, and resuspended in 900 µl of FCS + 100 µl of DMSO in cryotubes and stored at -80°C for 24 hours before transferring to a liquid nitrogen cell tank. As for the ASC hTERT 300 cells, after centrifugation, the cells were resuspended in the remaining medium and then mixed with 1ml of CryoStor® CS10 in cryotubes and kept at -80°C for 24 hours before transferring to a liquid nitrogen cell tank.

3.2.1. EV isolation

Once the ASC hTERT 300 cells reached ~ 80% confluence, the cells were conditioned in OptiMEM and incubated for 48 hours for the EVs accumulate in the supernatant (SN). The SN was then removed and centrifuged for 10 min at 2,000 x g to remove cell debris. Next, the SN was transferred to a vacuum filter (0,45 µm) and filtered through. To perform the tangential flow filtration (TFF), the membrane was first washed with NaOH to wash the protein remnants, then with ddH_2O, and ultimately with filtered DPBS. Next, the SN was poured into 50 ml syringes and pumped back and forth to manually pass through the TFF. The process continued until 10% of the initial volume had filtered through. Next, the TFF filter was washed with filtered DPBS, the filtrate transferred into 15 ml 10 kDa spin filters, and centrifuged at 2000 x g for 10 minutes to reach 300 µl of concentrate, which was ultimately aliquoted in low bind Eppendorf tubes and stored at -80°C. The concentrations of the isolated particle were then assessed via nanoparticle tracking analysis (NTA).

3.2.1. Nanoparticle tracking analysis (NTA)

To assess the concentration of the isolated EV samples, the ZetaView Quatt NTA was utilized by the application of 1:750 diluted samples in filtered DPBS. The EV samples were measured with a scatter sensitivity of 80 and a shutter value of 100 using the 488 nm laser as a light source. After the device auto-cleaning program, the sample chamber was further flushed with an additional 20 ml of ultra-pure water. Before sample measurement, the device had to be calibrated using 100 nm standard beads (Applied Microspheres, NanoStandards™-0.100 µm,75009-03), which were diluted 1:2500000

in ultra-pure water. After completing the calibration program, the system was flushed with 20 ml of sterile filtered DPBS before applying the diluted samples using a syringe. Additionally, a DPBS flush was carried out between each measurement.

3.2.1. Bicinchoninic Acid protein (BCA) Assay

The Pierce™ BCA protein kit was used to perform this assay. In brief, for the BCA protein assay in a microplate, the total volume of working reagent (WR) was calculated based on the number of samples, replicates, and assay volume. The WR was prepared by mixing BCA reagents A and B in a 50:1 ratio. Standards and unknown samples were added to wells, followed by WR, mixed, and incubated at 37°C. After cooling down to room temperature, the absorbance was measured at 562 nm. Blank readings were subtracted, and a standard curve was used to determine protein concentrations. The absorbance was measured at 560 nm via a POLARstar Omega plate reader. Ultimately, the concentrations were assessed using the standard curve, Fig. 6, as the reference.

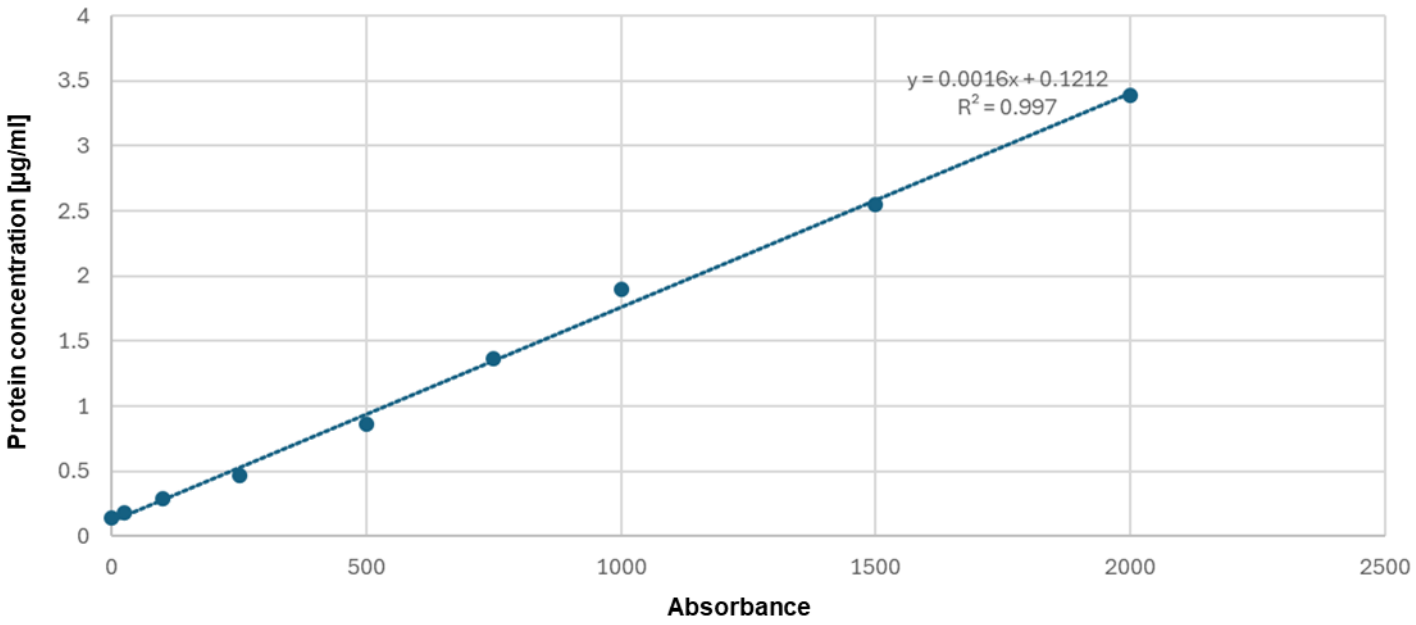

Figure 6 The standard curve used for the analysis of the BCA assay of the isolated EVs.

3.2.1. Dot Blot iodixanol density fractions

10 µl of each sample, diluted to match the concentration of the least concentrated sample, determined via a BCA assay, were incubated at 95°C to denature the proteins. Next, 2 µl of each sample was applied to its respective spot on a gridded cellulose membrane, and the membrane was dried on a heat block. The membrane was then incubated in 2% BSA-TBST for 1 hour at RT. Next, the membrane was cut into individual pieces, incubated in 10 ml of 1% BSA-TBST containing their respective HRP-conjugated antibodies, all diluted 1:1000 in TBST, namely, CD81 (mouse), TSG101 (rat), Syntenin-1 (mouse), and Calnexin (rabbit), and placed on a roller at 4°C overnight. In the next step, the membranes were washed in TBST 3x 5 minutes, incubated in HRP-conjugated secondary antibodies for 1h at RT, and washed again. Ultimately, the membrane was submerged in Clarity ECL substrate, incubated for 5 minutes, and imaged using a Chemidoc™ Imager.

3.2.2. AlamarBlue assay

10,000 BaF3 cells were seeded in 80 µl of medium per well in a 96-well plate. Next, $1*10^8$ EVs in 20 µl of each respective EV were added in 4 replicates. After 48 hours, 10 µl of alamarBlue reagent were added to each cell, incubated for 3h at 37°C, and the RFU values were examined by measuring fluorescence at excitation 544 nm and emission 590 nm wavelengths via an Omega plate reader.

3.2.1. MTT assay

Per well in a 96-well plate, 10,000 BaF3 cells were seeded in 80 µl of medium. Next, 20 µl of each respective EV construct containing $1*10^8$ EVs were added in 4 replicates. 48 hours after EV exposure,10 µl of MTT (5 mg/ml) were added to the cells. After 4 hours, 100 µl of lysis solution (10% SDS, 10 mM HCl) were added, and the cells were incubated at 4°C for 24 hours in the dark. Absorbance was measured at 570 nm in a plate reader. The measured data were corrected with the reference wavelength set at 650 nm and the blank. Subsequently, the results were normalized to the untreated sample.

3.2.2. Staining the EVs via CellMask™ Deep Red (CMDR)

The stock CMDR (diluted 1:20 in DMSO) was further diluted 1:5 in DPBS and ultimately 1:25/50 in the EV samples, each containing 1.5 × 10^8 EVs, resulting in a final CMDR concentration of 1 or 2 µg/µl. An additional sample containing CMDR in DPBS with no EVs was also prepared to serve as a background control. The EVs were then incubated in the dark for 30 minutes at RT. Next, the EVs were transferred to Amicon® Ultra 0.5 ml 10,000 centrifugal filter units and filled up to 500 µl with DPBS, centrifuged for 10 minutes at 10k x g at 4°C down to 100 µl, and collected in a collection tube. A washing step was followed to collect EVs stuck in the membrane. The stained EVs were then used for flow cytometry on the same day.

3.2.3. Flow cytometry

150,000-300,000 cells were transferred to sample tubes, centrifuged for 3 minutes at 500 x g, resuspended in 100 µl stained EVs for tracking and uptake into the cells, and incubated for 30 minutes in the dark. Next, the cells were either supplemented with 100 µl of 3x Trypsin-EDTA or 1% BSA /DPBS. Incubated for 5 minutes, followed by the addition of 1 ml cold 1% BSA/DPBS, and centrifuged for 3 minutes at 500 x g. A washing step was followed, and the cells were ultimately resuspended in 200 µl cold 1% BSA/DPBS, ready for the FC assay. Unstained and CMDR in DPBS controls were initially used to determine and adjust the gain and the gating. Next, the labeled cells were placed in the flow cytometer, and 10000 events were examined, and the results were recorded. Fig. 7 shows an example of the gating workflow carried out to assess the flow cytometry experiment results.

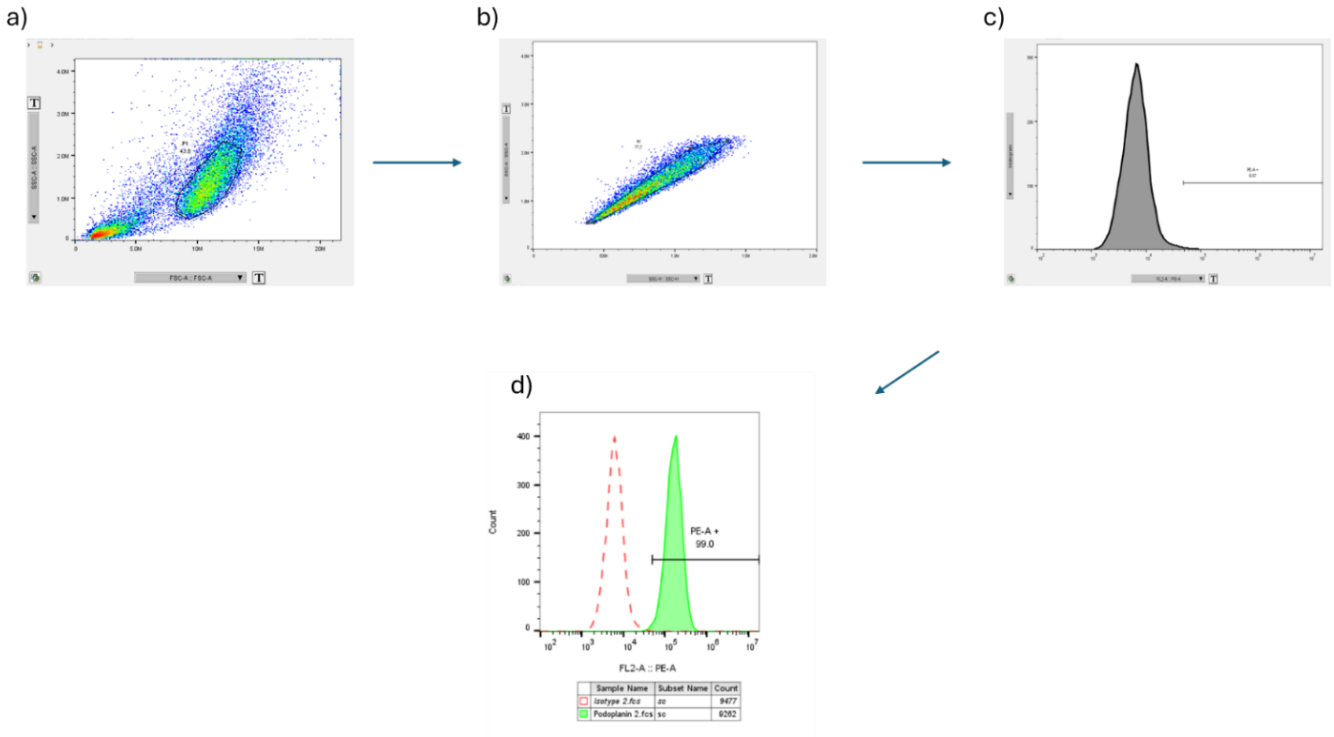

Figure 7 An example of the flow cytometry gating workflow.

a) SSC-A (side scatter area) over FSC-A (forward scatter area) to isolate cell populations b) SSC-A over SSC-H(height) plot to gate single cells c) A logarithmic histogram plot of the area of the PE (phycoerythrin) fluorescence signal from each event. A signal threshold of 0.5-1 is set on the isotype sample as the control to distinguish positive populations in the other samples d) Overlay of the histogram plots of isotype control and the other samples.

3.2.4. Scratch assay

HDLECs were grown to ~ 80% confluence. Using Ibidi culture insert 4 well in µ-dish 35 mm, 40,000 cells were seeded in each well with 100 µl EGM-2 medium, supplemented with rhVEGF-C and incubated at 37°C overnight. The next day, the inserts were removed with care, and the dishes were washed with DPBS. 1.5 ml of EGM-2, plus 50 µl EVs for the 3 samples: wildtype (WT), recombinant VEGF-C double construct, and recombinant VEGF-C single construct, were added to their respective dishes. Additionally, one dish contained cells in medium + 50 ng/ml rhVEGF-C as the positive control, and another dish contained untreated medium-only cells. Utilizing a microscope, images were taken at 0, 8, and 24-hour time points. These photos were then analyzed via ImageJ and the scratch assay plugin to measure the gap closure area, Fig. 13. Since the added EVs were of different concentrations, the net gap closure values of each sample were calculated by deducting the gap closure percentage of the medium-only sample, determined by comparison of the gap area at each timepoint to the initial 0-hour gap area set as 100%, from the stimulated samples

and then normalizing these values by dividing them by the total amount of protein added in µg, to ultimately achieve a normalized net gap closure percentage per µg of protein of each sample.

3.2.5. Statistical Analysis

The statistical analyses were carried out via GraphPad Prism 10. Normality of the data was tested via a Shapiro-Wilk test. Next, a Kruskal-Wallis test was utilized for not normally distributed and a one-way ANOVA for normally distributed data. Additionally, in WT normalized datasets, a one-sample t-test was utilized between WT and the engineered EV samples, where the hypothetical mean was set as 1. The specific tests are mentioned in the results section.

4. Results

4.1. Quantification of EV particle numbers

EV particle numbers were quantified by nanoparticle tracking analysis (NTA), Table 1, to ensure accurate comparison between samples.

Table 1 EV particle numbers of the engineered EVs assessed via NTA

EV sample	EV concentration (particles/ml)
WT	1.06E+08
Recombinant CD81-P1-VEGF-C single construct	7.40E+06
Recombinant CD81-P1-VEGF-C double construct	1.00E+07

4.2. Determination of EV protein concentrations

To assess the protein concentration of the engineered EVs for standardization in the subsequent experiments, such as dot blot assay, a BCA assay was carried out, Table 2.

Table 2 EV protein concentrations determined by BCA assay

EV sample	Concentration (µg/ml)
WT	7420
Recombinant CD81-P1-VEGF-C single construct	1985
Recombinant CD81-P1-VEGF-C double construct	8050

4.3. Enrichment of common EV markers in the EV samples

To characterize the isolated EVs, a dot blot assay was carried out to assess the presence of common EV markers in the EV isolates, such as CD81, TSG101, Syntenin-1, a dot blot assay was carried out. As shown in Fig. 8, all samples show signals for CD81, Syntenin-1, and faint signals for TSG101. All samples tested negative for Calnexin. A cell lysate cell sample would, however, be needed to validate the results as a positive control for the calnexin antibodies.

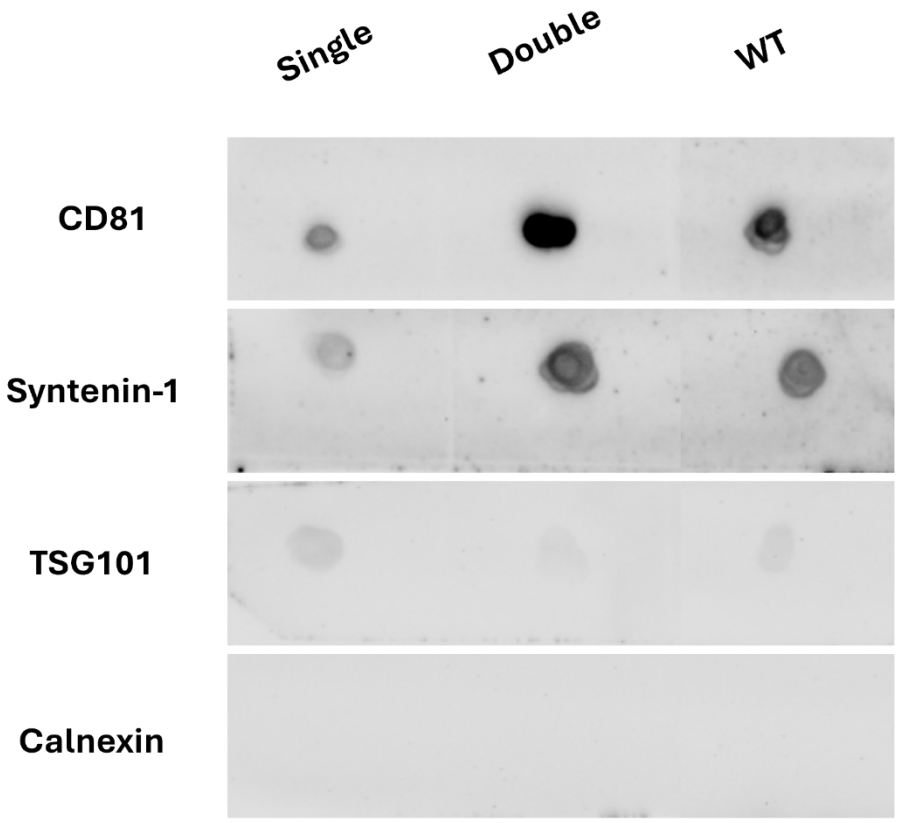

Figure 8 EV characterization via dot blot assay.

All samples show signals for CD81, Syntenin-1, and faint signals for TSG101. No signals were observed for Calnexin which served as the negative control in any of the samples. Single: CD81-P1-VEGF-C; Double: CD81-P1-VEGF-C/P1-VEGF-C

4.4. Improved cell proliferation of the engineered EVs

To evaluate the impact and effectiveness of the engineered EV constructs on cell proliferation, a series of alamarBlue assays were carried out on engineered BaF3 cells expressing chimeric VEGFR-3/EpoR receptors to study the changes in metabolic activity and cell proliferation of the samples supplemented with the engineered EVs and the WT sample in comparison to the cells cultured in medium with no additional supplements. As shown in Fig. 9, results show improved proliferation of the samples, normalized to the medium-only sample results after 48 hours of incubation with respective EVs. The recombinant double construct shows the highest increase in cell proliferation with a 2.2-fold change, followed by the recombinant VEGF-C single construct with 1.7-fold, the WT cells with 1.5-fold, and the soluble P1-VEGF-C sample

with 1.2-fold change in fluorescence intensity. The rhVEGF-C sample serving as the positive control in this experiment had a 3-fold increase in cell proliferation. Except for the double construct compared to the soluble P1-VEGF-C sample, the fold changes between the WT and the CD81 constructs were not significant.

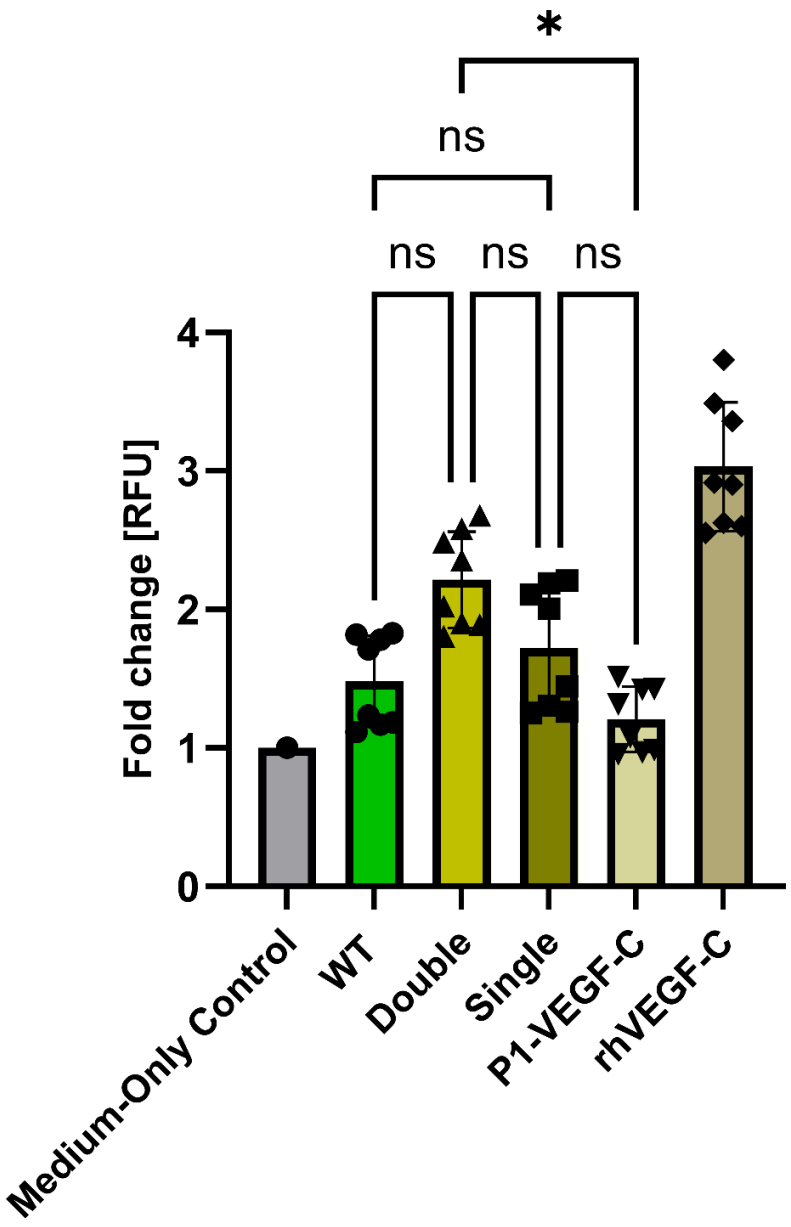

Figure 9 Metabolic activity of BaF3 cells assessed by alamarBlue assay.

*The results show improved cell proliferation of the samples, normalized to the medium-only control after 48h incubation with respective EVs.The recombiant CD81-P1-VEGF-C double construct shows the highest increase in cell proliferation with a 2.2-fold change, followed by the single construct with 1.7-fold, the WT cells with 1.5-fold, and the soluble P1-VEGF-C sample with 1.2 change. The rhVEGF-C sample serving as the positive control in this experiment had a 3-fold increase in cell proliferation. Kruskal-Wallis test was used for statistical analysis. Significance: * : p ≤ 0.05. Double: CD81-P1-VEGF-C/P1-VEGF-C; Single: CD81-P1-VEGF-C; RFU.: relative fluorescence units*

4.5. Recombinant VEGF-C single construct shows better binding and uptake with target cells

Utilizing CMDR staining and flow cytometry, the binding efficiency of the engineered EV constructs was assessed in 2 different cell types, namely BaF3 and HDLEC primary cells. To examine the EV uptake and the possible proteolytic effects of trypsin on the bound EVs, an additional set of cell samples was supplemented with 3x Trypsin-EDTA. The fold changes were calculated relative to the fluorescence intensity values of WT samples.

4.5.1. Enhanced recombinant VEGF-C single construct EV uptake and binding in BaF3 cells

As shown in Fig. 10, the recombinant CD81-P1-VEGF-C double construct shows a 13-fold increase, while the single construct sample shows a 30-fold increase in the fluorescence intensity compared to the untreated (trypsin –) WT. The trypsinized samples of recombinant CD81-P1-VEGF-C double construct and single constructs showed 11 and 26-fold increases in the fluorescence intensity, respectively. The trypsinized WT sample had a 0.8-fold change compared to the untreated WT. Both of the engineered constructs, with and without trypsin supplementation, showed significant increases in F.I. (fluorescence intensity) compared to the untreated WT. The untreated recombinant CD81-P1-VEGF-C single construct also showed a significant increase in F.I. compared to the untreated double construct.

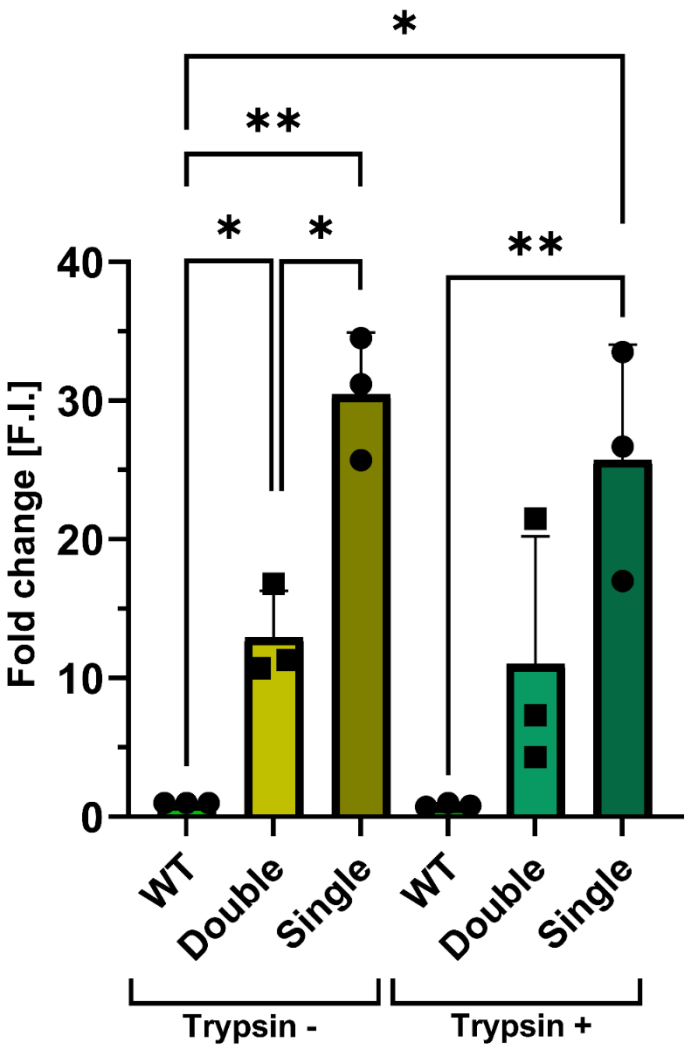

Figure 10 EV binding and uptake evaluation of BaF3 samples using Flow cytometry.

*The recombinant CD81-P1-VEGF-C double construct sample shows a 13-fold increase, and the single construct sample showed a 30-fold increase in the fluorescence intensity. The trypsinized samples of recombinant CD81-P1-VEGF-C double construct and the CD81-P1-VEGF-C single construct show 11 and 26-fold increase in the fluorescence intensity, respectively. The trypsinized WT sample had a 0.8-fold change compared to the untreated WT. All of the engineered constructs showed significant increases in F.I. compared to the trypsin (-) WT. The recombinant CD81-P1-VEGF-C single construct also showed a significant increase in F.I. compared to the recombinant CD81-P1-VEGF-C double construct. statistical analysis was carried out using one-sample t test and ordinary one-way ANOVA. Significance: * : $p \leq 0.05$, ** : ≤ 0.01. Double: CD81-P1-VEGF-C/P1-VEGF-C; Single: CD81-P1-VEGF-C; F.I.: fluorescence intensity .*

4.5.2. Enhanced recombinant VEGF-C single construct EV binding in HDLECs

As shown in Fig. 11, the recombinant VEGF-C double construct sample showed a 5-fold and the single construct sample showed a 21-fold increase in fluorescence intensity, both showing a significant increase compared to WT. The CD81 single construct also showed a significant increase in the fluorescent intensity compared to the double construct.

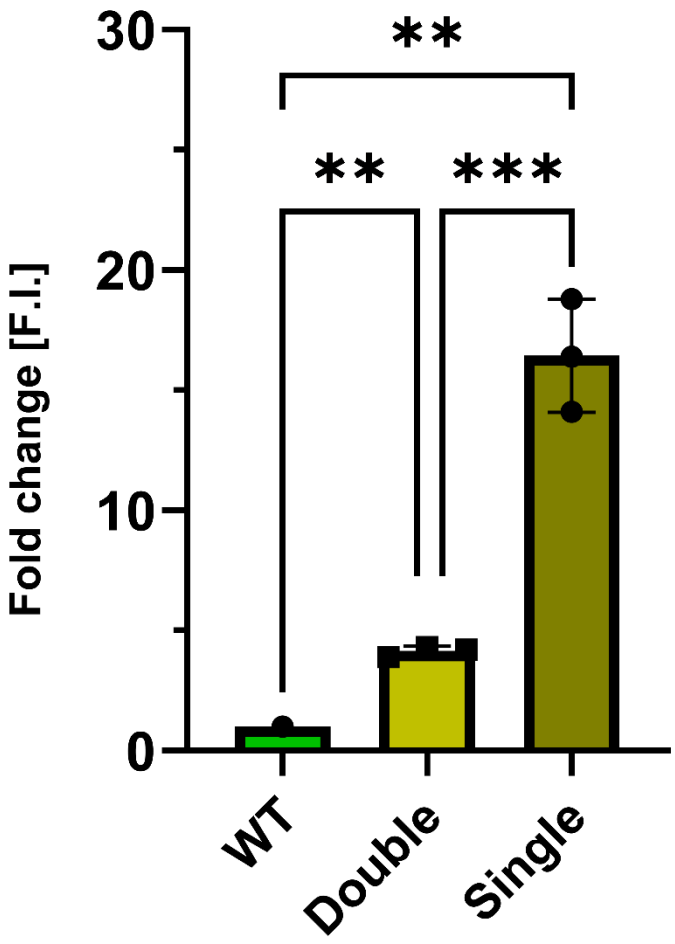

Figure 11 EV binding and uptake assessment of HDLECs via Flow cytometry.

*The recombinant VEGF-C double construct sample showed a 5-fold increase, and the single construct sample showed a 21-fold increase in fluorescence intensity, both showing a significant increase compared to WT. The CD81 single construct also showed a significant increase in the fluorescent intensity compared to the double construct. One-sample t-test and ordinary one-way ANOVA were used for the statistical analysis. Significance: * : p ≤ 0.05; **: ≤ 0.01;***: ≤ 0.001. Double: CD81-P1-VEGF-C/P1-VEGF-C; Single: CD81-P1-VEGF-C; F.I.: fluorescence intensity*

4.6. CD81-P1-VEGF-C single construct shows enhanced gap closure rate

Ultimately, a scratch assay was carried out to evaluate the gap closure efficacy of the EV constructs resulting from their ability to promote cell migration and proliferation in target HDLECs.

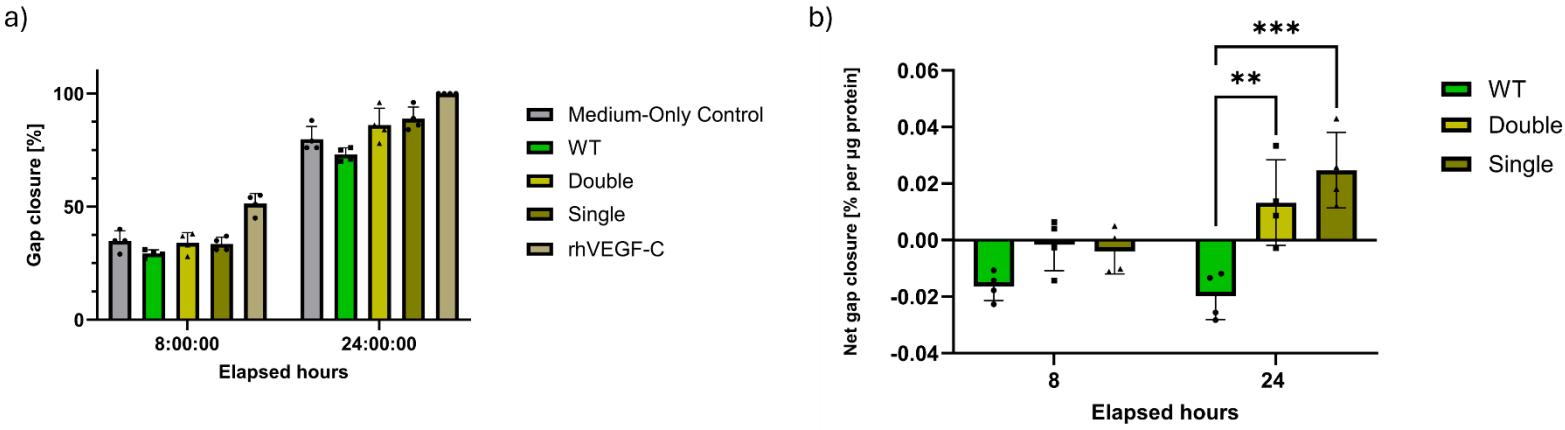

Figure 12 Gap closure efficiency evaluated via scratch assay.

*a) Gap closure percentage of the cells incubated with EVs in addition to medium-only control and rhVEGF-C positive control at the 8- and 24-hour timepoints. Compared to the medium-only sample with 34.8%, all of the samples, with the exception of rhVEGF-C positive control with 51.3%, had slower gap closure rates and showed a lower gap closure percentage at the 8-hour timepoint, with WT having the lowest rate with 29.3%, followed by the recombinant VEGF-C single construct with 33.5% and the recombinant VEGF-C double construct sample with 34 %. At the 24h timepoint, WT continued to have the lowest gap closure percentage with 73%. Whereas the medium-only control induced a 79.8% gap closure. The recombinant VEGF-C double and single constructs managed to surpass the medium-only control with gap closure percentages of 86 and 88.8, respectively. The rhVEGF-C sample induced a complete gap closure by the 24-hour timepoint. b) Net gap closure percentages of the EV-supplemented cells in comparison to the medium-only control and normalized to the amount of µg protein added to each sample. At the 8-hour timepoint, WT showed the lowest gap closure rate with -0.016%, followed by the recombinant VEGF-C double construct sample with -0.0016% and the recombinant VEGF-C single construct sample with -0.004. At the 24h timepoint, the WT continued to have an even lower gap closure % compared to the medium only sample with a -0.02% rate. The recombinant VEGF-C double and single constructs, however, had gap closure percentages of 0.0132 and 0.025, respectively. Both engineered constructs showed a significant increase in gap closure rates compared to the WT. statistical analysis was performed using ordinary one-way ANOVA. Significance: ; ** : p ≤ 0.01;*** : ≤ 0.001. Double: CD81-P1-VEGF-C/P1-VEGF-C; Single: CD81-P1-VEGF-C*

In comparison to the net gap closure percentage of the medium-only sample with 34.8%, as shown in Fig. 12a, all of the samples, excluding the rhVEGF-C positive control with 51.3%, had slower gap closure rates and showed a lower gap closure

percentage at the 8-hour timepoint, with WT having the lowest rate with 29.3%, followed by the recombinant VEGF-C single construct with 33.5% and the recombinant VEGF-C double construct sample with 34 %. At the 24-hour timepoint, WT continued to have the lowest gap closure percentage with 73%. Whereas the medium-only control induced a 79.8% gap closure. The recombinant VEGF-C double and single constructs managed to surpass the medium-only control with gap closure percentages of 86 and 88.8, respectively. The rhVEGF-C sample induced a complete gap closure by the 24-hour timepoint. Fig. 12b shows the net gap closure percentages of the EV-supplemented cells in comparison to the medium-only control and normalized to the amount of µg protein added to each sample. At the 8-hour timepoint, WT showed the lowest gap closure rate with -0.016%, followed by the recombinant VEGF-C double construct sample with -0.0016% and the recombinant VEGF-C single construct sample with -0.004. At the 24h timepoint, the WT continued to have an even lower gap closure percentage compared to the medium-only sample with a -0.02% rate. The recombinant VEGF-C double and single constructs, however, had gap closure percentages of 0.0132 and 0.025, respectively. Both engineered constructs showed a significant increase in gap closure rates compared to the WT. Microscope images of the sample are presented in Fig. 13.

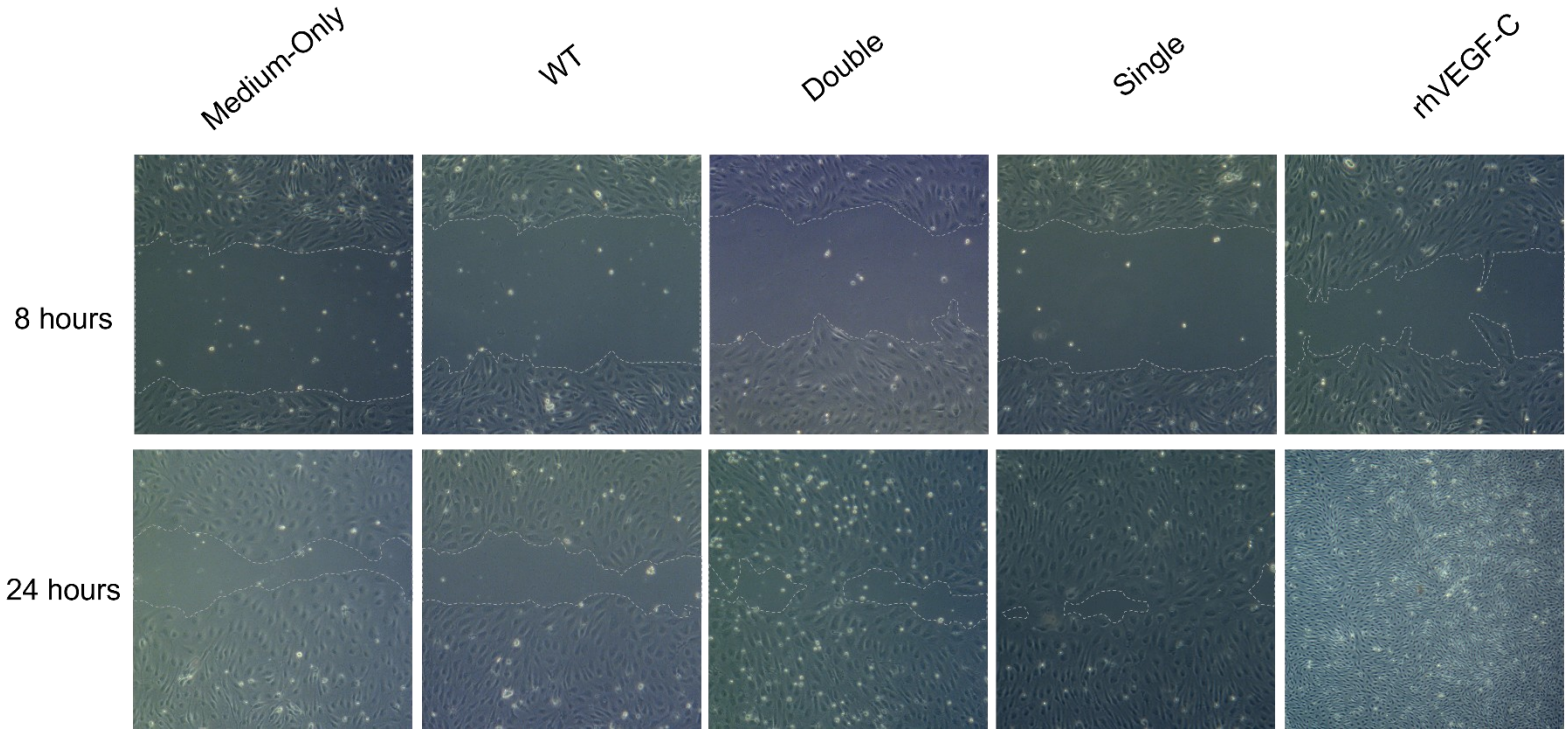

Figure 13 Scratch assay images of the samples at 8- and 24-hour timepoints.

The measured gap area is within the marked dashed lines. Double: CD81-P1-VEGF-C/P1-VEGF-C; Single: CD81-P1-VEGF-C

5. Discussion

The dot blot assay, Fig. 8, showed the presence of CD81 and Synthenin-1, which were in line with expectations, as these markers are amongst the most abundant EV-associated proteins in various cell types, including ASC hTERT 300 cells from which the EVs were isolated [69]. TSG101 is another common EV marker, more specifically in exosomes [70], which does appear in all the samples, although with a lower intensity. As for the negative control of the dot blot assay, all the samples tested negative for calnexin, an endoplasmic reticulum membrane protein, not typically present in EVs [71]. The results suggest successful enrichment of the common EV markers. To verify these results, specifically for calnexin as the negative control in this experiment, a cell lysate sample should have also been included as the positive control for calnexin.

The alamarBlue assay results, Fig.9, show the recombinant CD81-P1-VEGF-C double construct having the strongest fluorescence intensity, which indicates the highest proliferation of the cells, followed by recombinant CD81-P1-VEGF-C single construct, WT, and soluble P1-VEGF-C, relative to the untreated sample. The lower fluorescence intensity values of the soluble P1-VEGF-C sample, especially in comparison to WT, would suggest the instability of the protein, which results in its inability to trigger receptor activation and the subsequent cell proliferation. Both recombinant CD81 EV constructs show improvements in cell proliferation in comparison to WT. In contrast, the flow cytometry results for both tested cell types, BaF3 and HDLEC primary cells, shown in Figures 10 and 11, revealed an opposite trend between the double and single constructs, where the single construct EVs exhibited the highest fluorescence intensity. Both samples demonstrated significantly improved cell-binding and uptake capabilities compared to WT, as indicated by the fluorescence values. Between the trypsinized and trypsin (–) BaF3 sample sets, a reduction in fluorescence intensity was observed, which would indicate the dissociation of surface-bound EVs in the trypsinized samples and the recorded signal originating solely from internalized EVs. However, these changes were not statistically significant; hence, the trypsinization was not continued with the HDLECs. Other conditions, such as incubating the cells with the EVs at 4 °C during the cell labeling step, would prevent EV endocytosis and allow the distinction between solely bound and internalized EVs [72]. Imaging via a fluorescence microscope would also allow visualization of the bound EVs. The fold change trend between the

recombinant CD81 constructs was observed in both cell types. However, the relative fluorescence intensity fold change compared to WT was stronger in the BaF3 cells. The fold change ratio between the two EV constructs remained relatively unchanged with the addition of trypsin, compared to no trypsin.

Based on these results, the recombinant CD81-P1-VEGF-C single construct EVs have the highest cell binding and uptake efficiency, yet prove to be less effective in increasing cell proliferation in comparison to the CD81-P1-VEGF-C double construct. This suggests that while the single construct exhibits higher binding efficiency compared to the double construct, it falls short in terms of receptor binding and activation. A possible cause would be the random dimerization of the single construct EVs with each other via their CD81-bound VEGF-C proteins, which, on one hand, prevents receptor binding and, on the other hand, clusters the EVs together, leading to a higher fluorescence signal when interacting with the cell membrane. To examine this hypothesis, another experiment design where the tested cells lack VEGFR-3 would elucidate if the EV binding and uptake is, in fact receptor-specific or via other pathways such as phagocytosis, macropinocytosis, or direct fusion, which don't require receptor activation. Another factor that should be taken into account is the higher protein concentration of the double construct EVs compared to the single construct EVs, as shown in Table. 2, is around 4-fold higher, which can be a contributing factor for the increased cell proliferation. Hence, another alamarBlue assay where the amount of added EVs is standardized to the particle count, but to the protein concentration, would help elucidate the proliferative enhancement capabilities of the engineered EVs.

Regarding the scratch assay, the interpretation of the results is faced with limitations, as the number of supplemented EVs varied in each sample, with the WT sample having received around 10-fold the number of EVs compared to the engineered EVs. The plot in Fig. 12a shows the gap closure percentages prior to the normalization of the cells to the added protein amount, where the trend between the EV-supplemented cells can still be observed. The plot shown in Fig. 12b demonstrates the net closure percentage per µg of protein, which was carried out in this manner to optimally normalize the data despite the unequal EV supplementation. Based on these results, the two recombinant CD81-P1-VEGFC constructs start off with a disadvantage at the 8-hour time point, having slower gap closure percentages compared to the untreated cells in the medium-only sample, but manage to surpass it after 24 hours, with the single construct being

twice as efficient as the double construct. When taking these results at face value, the engineered EVs display a significant increase in gap closure ability in comparison to the WT, which proved to be even slower than untreated cells, yet again showcasing the potential of these engineered EVs. These results, however, must be validated by another experiment in which the samples are incubated with an equal number of EVs before any concrete interpretations and claims can be made. Considering the results from the alamarBlue and flow cytometry assays, in the case of BaF3 cells, the recombinant single construct appears to be better at binding to the cells but not as efficient in improving cell proliferation and metabolic activity compared to the recombinant double construct EVs. As for the HDLECs, the results from the scratch assay and the flow cytometry assay demonstrate recombinant VEGF-C single construct having not only a higher fluorescence intensity and better cell binding in the flow cytometry assay, but a higher gap closure efficacy in the scratch assay as well. It is worth noting that although cell proliferation is an important factor in both alamarBlue and scratch assays, cell migration also plays a significant role in the scratch assay. Moreover, the cells used in the alamarBlue assay, and the scratch assay were not of the same type, hence a direct comparison of these assays would not be plausible. To solve this issue, either an alamarBlue assay with the HDLECs or a scratch assay with the BaF3 cells would be essential to be able to conduct an accurate comparison. A BrdU assay would also be a suitable technique to further evaluate and compare the cell proliferation rates of the samples.

In conclusion, both recombinant CD81-P1-VEGF-C constructs show a strong increase in cell binding and uptake, proliferation, and migration compared to WT in all conducted experiments, which is a promising factor and improvement for further research and future therapeutic usage of these EV constructs; however, this would be subject to further validations. To further expand our understanding and the effects of these engineered EVs, experiments, such as live imaging flow cytometry to assess the EV uptake, Matrigel assay for angiogenesis analyses, alamarBlue and scratch assays with cells lacking VEGFR-3 expression for binding specificity of the EVs and ultimately, in vivo tests such as Matrigel plug assay could be performed to examine how the EVs impact the cells in a host/*in vivo* setting.

While other methods, such as ASC transplantation, have been investigated as a therapeutic method to target secondary lymphedema, yielding positive results [73],

there are also concerns about the possible tumorigenic effects of ASCs in patients [74] This potential oncogenic risk can, however, be reduced by the utilization of ASC-EVs, as they lack cellular replication capacity [75], while still providing beneficial effects and improvements in lymphangiogenesis and Lymphedema. [76] A challenge faced by EV-based therapeutics is the limited targeting capability of unmodified EVs, which has proven insufficient for clinical applications [77][78][79]. As mentioned earlier, however, the possibility to bioengineer EV composition, more specifically the surface proteins, offers vast opportunities to fine-tune the homing of EVs for each respective target cell. In case of LECs and Lymphedema, a recent study [80], has reported significant improvements in tube formation, proliferation, migration of LECs by utilizing engineered exosomes overexpressing CD63-VEGF-C fusion protein on the EV membrane. This study also claimed that the incorporation of these CD63-VEGFC exosomes in sodium alginate hydrogel significantly improved lymphedema in an acquired mouse tail lymphedema model. A major limitation with this experimental setup and the utilized CD63 construct, however, is that by directly fusing the VEGF-C to the CD63, not only would the VEGF-C not be presented extracellularly on the surface of the EV, but it could also disrupt the structure and function of CD63, and would consequently not lead to the intended effects and results the authors claim. This issue yet again highlights the relevance of the snorkel tag system, where fusing a VEGF-C-presenting snorkel tag onto CD81 would ensure the extracellular presentation of VEGF-C. This structural separation could also enhance the binding of VEGF-C to VEGFR-3, as the VEGF-C would encounter less steric hindrance and facilitate the affinity purification of EVs from complex matrices in a non-destructive manner while preserving their structural and functional integrity.

Ultimately, EVs engineered using the snorkel tag system hold great potential for precise and effective therapies across a wide range of diseases and conditions, as they allow versatile, targeted modifications and tailored designs to enhance therapeutic efficacy and tissue homing. As with any other novel system, however, the full extent and therapeutic potential of this approach remain to be further studied and scientifically validated in future research.

6. References

[1] G. M. Nelson, T. P. Padera, I. Garkavtsev, T. Shioda, and R. K. Jain, “Differential Gene Expression of Primary Cultured Lymphatic and Blood Vascular Endothelial Cells,” *Neoplasia*, vol. 9, no. 12, pp. 1038–1045, Dec. 2007, doi: 10.1593/neo.07643.

[2] G. J. Randolph, S. Ivanov, B. H. Zinselmeyer, and J. P. Scallan, “The Lymphatic System: Integral Roles in Immunity,” *Annu Rev Immunol*, vol. 35, no. 1, pp. 31–52, Apr. 2017, doi: 10.1146/annurev-immunol-041015-055354.

[3] M. K. Pugsley and R. Tabrizchi, “The vascular system,” *J Pharmacol Toxicol Methods*, vol. 44, no. 2, pp. 333–340, Sep. 2000, doi: 10.1016/S1056-8719(00)00125-8.

[4] G. Oliver, J. Kipnis, G. J. Randolph, and N. L. Harvey, “The Lymphatic Vasculature in the 21st Century: Novel Functional Roles in Homeostasis and Disease,” *Cell*, vol. 182, no. 2, pp. 270–296, Jul. 2020, doi: 10.1016/j.cell.2020.06.039.

[5] G. Guven, M. P. Hilty, and C. Ince, “Microcirculation: Physiology, Pathophysiology, and Clinical Application,” *Blood Purif*, vol. 49, no. 1–2, pp. 143–150, 2020, doi: 10.1159/000503775.

[6] A. A. Grada and T. J. Phillips, “Lymphedema: Pathophysiology and clinical manifestations,” *J Am Acad Dermatol*, vol. 77, no. 6, pp. 1009–1020, Dec. 2017, doi: 10.1016/J.JAAD.2017.03.022.

[7] S. Simeroth and P. Yu, “The role of lymphatic endothelial cell metabolism in lymphangiogenesis and disease,” *Front Cardiovasc Med*, vol. 11, May 2024, doi: 10.3389/fcvm.2024.1392816.

[8] S. Banerji *et al.*, “LYVE-1, a New Homologue of the CD44 Glycoprotein, Is a Lymph-specific Receptor for Hyaluronan,” *J Cell Biol*, vol. 144, no. 4, pp. 789–801, Feb. 1999, doi: 10.1083/jcb.144.4.789.

[9] M. Pultar *et al.*, “Analysis of extracellular vesicle microRNA profiles reveals distinct blood and lymphatic endothelial cell origins,” *Journal of Extracellular Biology*, vol. 3, no. 1, Jan. 2024, doi: 10.1002/jex2.134.

[10] T. Tammela and K. Alitalo, “Lymphangiogenesis: Molecular Mechanisms and Future Promise,” *Cell*, vol. 140, no. 4, pp. 460–476, Feb. 2010, doi: 10.1016/j.cell.2010.01.045.

[11] B. C. Sleigh and B. Manna, *Lymphedema*. 2025.

[12] P. Brouillard *et al.*, “Primary lymphoedema,” *Nat Rev Dis Primers*, vol. 7, no. 1, p. 77, Oct. 2021, doi: 10.1038/s41572-021-00309-7.

[13] L. J. Greenspan and B. M. Weinstein, “To be or not to be: endothelial cell plasticity in development, repair, and disease,” *Angiogenesis*, vol. 24, no. 2, pp. 251–269, May 2021, doi: 10.1007/s10456-020-09761-7.

[14] N. Ferrara, “VEGF and Intraocular Neovascularization: From Discovery to Therapy.,” *Transl Vis Sci Technol*, vol. 5, no. 2, p. 10, Mar. 2016, doi: 10.1167/tvst.5.2.10.

[15] M. Shibuya, “Vascular Endothelial Growth Factor (VEGF) and Its Receptor (VEGFR) Signaling in Angiogenesis: A Crucial Target for Anti- and Pro-Angiogenic Therapies.,” *Genes Cancer*, vol. 2, no. 12, pp. 1097–105, Dec. 2011, doi: 10.1177/1947601911423031.

[16] C. Lee, M.-J. Kim, A. Kumar, H.-W. Lee, Y. Yang, and Y. Kim, “Vascular endothelial growth factor signaling in health and disease: from molecular mechanisms to therapeutic perspectives,” *Signal Transduct Target Ther*, vol. 10, no. 1, p. 170, May 2025, doi: 10.1038/s41392-025-02249-0.

[17] F. Zhang *et al.*, “VEGF-B is dispensable for blood vessel growth but critical for their survival, and VEGF-B targeting inhibits pathological angiogenesis,” *Proceedings of the National Academy of Sciences*, vol. 106, no. 15, pp. 6152–6157, Apr. 2009, doi: 10.1073/pnas.0813061106.

[18] R. Mallick *et al.*, “VEGF-B is a novel mediator of ER stress which induces cardiac angiogenesis via RGD-binding integrins independent of VEGFR1/NRP activities.,” *Mol Ther*, vol. 33, no. 7, pp. 3242–3256, Jul. 2025, doi: 10.1016/j.ymthe.2025.03.012.

[19] D. I. R. Holmes and I. Zachary, “The vascular endothelial growth factor (VEGF) family: angiogenic factors in health and disease.,” *Genome Biol*, vol. 6, no. 2, p. 209, 2005, doi: 10.1186/gb-2005-6-2-209.

[20] V. Joukov *et al.*, “Proteolytic processing regulates receptor specificity and activity of VEGF-C.,” *EMBO J*, vol. 16, no. 13, pp. 3898–911, Jul. 1997, doi: 10.1093/emboj/16.13.3898.

[21] B. K. McColl *et al.*, “Plasmin Activates the Lymphangiogenic Growth Factors VEGF-C and VEGF-D,” *J Exp Med*, vol. 198, no. 6, pp. 863–868, Sep. 2003, doi: 10.1084/jem.20030361.

[22] M. G. Achen *et al.*, “Vascular endothelial growth factor D (VEGF-D) is a ligand for the tyrosine kinases VEGF receptor 2 (Flk1) and VEGF receptor 3 (Flt4).,” *Proc Natl Acad Sci U S A*, vol. 95, no. 2, pp. 548–53, Jan. 1998, doi: 10.1073/pnas.95.2.548.

[23] K. Chau, A. Hennessy, and A. Makris, “Placental growth factor and pre-eclampsia,” *J Hum Hypertens*, vol. 31, no. 12, pp. 782–786, Dec. 2017, doi: 10.1038/jhh.2017.61.

[24] M. Lohela, M. Bry, T. Tammela, and K. Alitalo, “VEGFs and receptors involved in angiogenesis versus lymphangiogenesis,” *Curr Opin Cell Biol*, vol. 21, no. 2, pp. 154–165, Apr. 2009, doi: 10.1016/j.ceb.2008.12.012.

[25] N. Ferrara, “Vascular Endothelial Growth Factor: Basic Science and Clinical Progress,” *Endocr Rev*, vol. 25, no. 4, pp. 581–611, Aug. 2004, doi: 10.1210/er.2003-0027.

[26] R. S. Apte, D. S. Chen, and N. Ferrara, “VEGF in Signaling and Disease: Beyond Discovery and Development,” *Cell*, vol. 176, no. 6, pp. 1248–1264, Mar. 2019, doi: 10.1016/j.cell.2019.01.021.

[27] K. Pajusola *et al.*, “FLT4 receptor tyrosine kinase contains seven immunoglobulin-like loops and is expressed in multiple human tissues and cell lines.,” *Cancer Res*, vol. 52, no. 20, pp. 5738–43, Oct. 1992.

[28] I. Zachary, “Neuropilins: Role in Signalling, Angiogenesis and Disease,” 2014, pp. 37–70. doi: 10.1159/000354169.

[29] P. M. Calvo, R. G. Hernández, A. M. Pastor, and R. R. de la Cruz, “VEGF and Neuronal Survival,” *The Neuroscientist*, vol. 30, no. 1, pp. 71–86, Feb. 2024, doi: 10.1177/10738584221120803.

[30] M. J. Karkkainen and K. Alitalo, “Lymphatic endothelial regulation, lymphoedema, and lymph node metastasis,” *Semin Cell Dev Biol*, vol. 13, no. 1, pp. 9–18, Feb. 2002, doi: 10.1006/scdb.2001.0286.

[31] G. Siegfried *et al.*, “The secretory proprotein convertases furin, PC5, and PC7 activate VEGF-C to induce tumorigenesis,” *Journal of Clinical Investigation*, vol. 111, no. 11, pp. 1723–1732, Jun. 2003, doi: 10.1172/JCI17220.

[32] V. Joukov *et al.*, “Proteolytic processing regulates receptor specificity and activity of VEGF-C,” *EMBO J*, vol. 16, no. 13, pp. 3898–3911, Jul. 1997, doi: 10.1093/emboj/16.13.3898.

[33] B. K. McColl *et al.*, “Plasmin Activates the Lymphangiogenic Growth Factors VEGF-C and VEGF-D,” *J Exp Med*, vol. 198, no. 6, pp. 863–868, Sep. 2003, doi: 10.1084/jem.20030361.

[34] A. Salameh, F. Galvagni, M. Bardelli, F. Bussolino, and S. Oliviero, “Direct recruitment of CRK and GRB2 to VEGFR-3 induces proliferation, migration, and survival of endothelial cells through the activation of ERK, AKT, and JNK pathways,” *Blood*, vol. 106, no. 10, pp. 3423–3431, Nov. 2005, doi: 10.1182/blood-2005-04-1388.

[35] T. Makinen, “Isolated lymphatic endothelial cells transduce growth, survival and migratory signals via the VEGF-C/D receptor VEGFR-3,” *EMBO J*, vol. 20, no. 17, pp. 4762–4773, Sep. 2001, doi: 10.1093/emboj/20.17.4762.

[36] Y. Deng, X. Zhang, and M. Simons, “Molecular Controls of Lymphatic VEGFR3 Signaling,” *Arterioscler Thromb Vasc Biol*, vol. 35, no. 2, pp. 421–429, Feb. 2015, doi: 10.1161/ATVBAHA.114.304881.

[37] K. G. Kuonqui *et al.*, “Regulation of VEGFR3 signaling in lymphatic endothelial cells,” *Front Cell Dev Biol*, vol. 13, Feb. 2025, doi: 10.3389/fcell.2025.1527971.

[38] Y. Guo, W. Pan, S. Liu, Z. Shen, Y. Xu, and L. Hu, “ERK/MAPK signalling pathway and tumorigenesis (Review),” *Exp Ther Med*, Jan. 2020, doi: 10.3892/etm.2020.8454.

[39] L. C. Dieterich *et al.*, “DeepCAGE Transcriptomics Reveal an Important Role of the Transcription Factor MAFB in the Lymphatic Endothelium,” *Cell Rep*, vol. 13, no. 7, pp. 1493–1504, Nov. 2015, doi: 10.1016/j.celrep.2015.10.002.

[40] J.-L. Su *et al.*, “The role of the VEGF-C/VEGFR-3 axis in cancer progression,” *Br J Cancer*, vol. 96, no. 4, pp. 541–545, Feb. 2007, doi: 10.1038/sj.bjc.6603487.

[41] T. Makinen, “Isolated lymphatic endothelial cells transduce growth, survival and migratory signals via the VEGF-C/D receptor VEGFR-3,” *EMBO J*, vol. 20, no. 17, pp. 4762–4773, Sep. 2001, doi: 10.1093/emboj/20.17.4762.

[42] N. Beheshtizadeh *et al.*, “Vascular endothelial growth factor (VEGF) delivery approaches in regenerative medicine,” *Biomedicine & Pharmacotherapy*, vol. 166, p. 115301, Oct. 2023, doi: 10.1016/j.biopha.2023.115301.

[43] A. Szuba *et al.*, “Therapeutic lymphangiogenesis with human recombinant VEGF-C,” *The FASEB Journal*, vol. 16, no. 14, pp. 1985–1987, Dec. 2002, doi: 10.1096/fj.02-0401fje.

[44] S. Schwager *et al.*, “Antibody-mediated delivery of VEGF-C potently reduces chronic skin inflammation.,” *JCI Insight*, vol. 3, no. 23, Dec. 2018, doi: 10.1172/jci.insight.124850.

[45] D. Szőke *et al.*, “Nucleoside-modified VEGFC mRNA induces organ-specific lymphatic growth and reverses experimental lymphedema,” *Nat Commun*, vol. 12, no. 1, p. 3460, Jun. 2021, doi: 10.1038/s41467-021-23546-6.

[46] J. Mondal *et al.*, “Hybrid exosomes, exosome-like nanovesicles and engineered exosomes for therapeutic applications,” *Journal of Controlled Release*, vol. 353, pp. 1127–1149, Jan. 2023, doi: 10.1016/j.jconrel.2022.12.027.

[47] F. U. Rehman, Y. Liu, M. Zheng, and B. Shi, “Exosomes based strategies for brain drug delivery,” *Biomaterials*, vol. 293, p. 121949, Feb. 2023, doi: 10.1016/j.biomaterials.2022.121949.

[48] M. P. Zaborowski, L. Balaj, X. O. Breakefield, and C. P. Lai, “Extracellular Vesicles: Composition, Biological Relevance, and Methods of Study,” *Bioscience*, vol. 65, no. 8, pp. 783–797, Aug. 2015, doi: 10.1093/biosci/biv084.

[49] L. Doyle and M. Wang, “Overview of Extracellular Vesicles, Their Origin, Composition, Purpose, and Methods for Exosome Isolation and Analysis,” *Cells*, vol. 8, no. 7, p. 727, Jul. 2019, doi: 10.3390/cells8070727.

[50] C. Théry *et al.*, “Minimal information for studies of extracellular vesicles 2018 (MISEV2018): a position statement of the International Society for Extracellular Vesicles and update of the MISEV2014 guidelines,” *J Extracell Vesicles*, vol. 7, no. 1, Dec. 2018, doi: 10.1080/20013078.2018.1535750.

[51] A. Milasan, N. Tessandier, S. Tan, A. Brisson, E. Boilard, and C. Martel, “Extracellular vesicles are present in mouse lymph and their level differs in atherosclerosis,” *J Extracell Vesicles*, vol. 5, no. 1, Jan. 2016, doi: 10.3402/jev.v5.31427.

[52] L. A. Mulcahy, R. C. Pink, and D. R. F. Carter, “Routes and mechanisms of extracellular vesicle uptake,” *J Extracell Vesicles*, vol. 3, no. 1, Jan. 2014, doi: 10.3402/jev.v3.24641.

[53] A. Samii and F. Razmkhah, “Transformation of Hematopoietic Stem and Progenitor Cells by Leukemia Extracellular Vesicles: A Step Toward Leukemogenesis,” *Stem Cell Rev Rep*, vol. 16, no. 6, pp. 1081–1091, Dec. 2020, doi: 10.1007/s12015-020-09975-8.

[54] E. Bonsergent, E. Grisard, J. Buchrieser, O. Schwartz, C. Théry, and G. Lavieu, “Quantitative characterization of extracellular vesicle uptake and content delivery within mammalian cells,” *Nat Commun*, vol. 12, no. 1, p. 1864, Mar. 2021, doi: 10.1038/s41467-021-22126-y.

[55] M. J. Haney *et al.*, “Exosomes as drug delivery vehicles for Parkinson’s disease therapy,” *Journal of Controlled Release*, vol. 207, pp. 18–30, Jun. 2015, doi: 10.1016/j.jconrel.2015.03.033.

[56] X. Liang *et al.*, “Engineering of extracellular vesicles for efficient intracellular delivery of multimodal therapeutics including genome editors,” *Nature Communications* , vol. 16, no. 1, Dec. 2025, doi: 10.1038/s41467-025-59377-y.

[57] Z. Li *et al.*, “Advancements in extracellular vesicles biomanufacturing: a comprehensive overview of large-scale production and clinical research,” *Front Bioeng Biotechnol*, vol. 13, Feb. 2025, doi: 10.3389/fbioe.2025.1487627.

[58] A. M. Zickler *et al.*, “Novel Endogenous Engineering Platform for Robust Loading and Delivery of Functional mRNA by Extracellular Vesicles,” *Advanced Science*, vol. 11, no. 42, Nov. 2024, doi: 10.1002/advs.202407619.

[59] M. Brown *et al.*, “Snorkel: An Epitope Tagging System for Measuring the Surface Expression of Membrane Proteins,” *PLoS One*, vol. 8, no. 9, p. e73255, Sep. 2013, doi: 10.1371/journal.pone.0073255.

[60] M. R. Bobbili *et al.*, “Snorkel-tag based affinity chromatography for recombinant extracellular vesicle purification,” *J Extracell Vesicles*, vol. 13, no. 10, Oct. 2024, doi: 10.1002/jev2.12523.

[61] M. R. Tardif and M. J. Tremblay, “Tetraspanin CD81 Provides a Costimulatory Signal Resulting in Increased Human Immunodeficiency Virus Type 1 Gene Expression in Primary CD4 + T Lymphocytes through NF-κB, NFAT, and AP-1 Transduction Pathways,” *J Virol*, vol. 79, no. 7, pp. 4316–4328, Apr. 2005, doi: 10.1128/JVI.79.7.4316-4328.2005.

[62] N. Labusek *et al.*, “Extracellular vesicles from immortalized mesenchymal stromal cells protect against neonatal hypoxic-ischemic brain injury.,” *Inflamm Regen*, vol. 43, no. 1, p. 24, Apr. 2023, doi: 10.1186/s41232-023-00274-6.

[63] S. Wolbank *et al.*, “*Telomerase* Immortalized Human Amnion- and Adipose-Derived Mesenchymal Stem Cells: Maintenance of Differentiation and Immunomodulatory

Characteristics," *Tissue Eng Part A*, vol. 15, no. 7, pp. 1843–1854, Jul. 2009, doi: 10.1089/ten.tea.2008.0205.

[64] J.-H. Wang, X.-L. Liu, J.-M. Sun, J.-H. Yang, D.-H. Xu, and S.-S. Yan, "Role of mesenchymal stem cell derived extracellular vesicles in autoimmunity: A systematic review," *World J Stem Cells*, vol. 12, no. 8, pp. 879–896, Aug. 2020, doi: 10.4252/wjsc.v12.i8.879.

[65] T. Kim, J. W. Hong, and L. P. Lee, "Efficient methods of isolation and purification of extracellular vesicles.," *Nano Converg*, vol. 12, no. 1, p. 45, Sep. 2025, doi: 10.1186/s40580-025-00509-x.

[66] X. Zheng *et al.*, "Small extracellular vesicles purification and scale-up," *Front Immunol*, vol. 15, Feb. 2024, doi: 10.3389/fimmu.2024.1344681.

[67] S. Yang *et al.*, "A New Large-Scale Extracellular Vesicle Production Strategy for Biomedical Drug Development," Apr. 19, 2024. doi: 10.1101/2024.04.15.589541.

[68] K. M. McKinnon, "Flow Cytometry: An Overview," *Curr Protoc Immunol*, vol. 120, no. 1, Jan. 2018, doi: 10.1002/cpim.40.

[69] C. Gorgun *et al.*, "Role of Extracellular Vesicles from Adipose Tissue- and Bone Marrow-Mesenchymal Stromal Cells in Endothelial Proliferation and Chondrogenesis," *Stem Cells Transl Med*, vol. 10, no. 12, pp. 1680–1695, Dec. 2021, doi: 10.1002/sctm.21-0107.

[70] Z. Zhou, Y. Tao, H. Zhao, and Q. Wang, "Adipose Extracellular Vesicles: Messengers From and to Macrophages in Regulating Immunometabolic Homeostasis or Disorders," *Front Immunol*, vol. 12, May 2021, doi: 10.3389/fimmu.2021.666344.

[71] M. I. Ramirez *et al.*, "Technical challenges of working with extracellular vesicles," *Nanoscale*, vol. 10, no. 3, pp. 881–906, 2018, doi: 10.1039/C7NR08360B.

[72] E. Bonsergent, E. Grisard, J. Buchrieser, O. Schwartz, C. Théry, and G. Lavieu, "Quantitative characterization of extracellular vesicle uptake and content delivery within mammalian cells," *Nat Commun*, vol. 12, no. 1, p. 1864, Mar. 2021, doi: 10.1038/s41467-021-22126-y.

[73] R. Ogino, K. Hayashida, S. Yamakawa, and E. Morita, "Adipose-Derived Stem Cells Promote Intussusceptive Lymphangiogenesis by Restricting Dermal Fibrosis in Irradiated Tissue of Mice.," *Int J Mol Sci*, vol. 21, no. 11, May 2020, doi: 10.3390/ijms21113885.

[74] Y. W. Chan *et al.*, “Adipose-derived stem cells and cancer cells fuse to generate cancer stem cell-like cells with increased tumorigenicity,” *J Cell Physiol*, vol. 235, no. 10, pp. 6794–6807, Oct. 2020, doi: 10.1002/jcp.29574.

[75] S. Han, J. Cai, Y. Zhang, and F. Lu, “Mesenchymal stem cell therapy for breast cancer-related secondary lymphedema (Review),” *Mol Clin Oncol*, vol. 23, no. 2, pp. 1–13, Jun. 2025, doi: 10.3892/mco.2025.2868.

[76] K. Tashiro, Y. Yoshioka, and T. Ochiya, “Extracellular Vesicles from Adipose-Derived Stem Cells Relieve Extremity Lymphedema in Mouse Models.,” *Plast Reconstr Surg*, vol. 152, no. 5, pp. 1011–1021, Nov. 2023, doi: 10.1097/PRS.0000000000010388.

[77] L. Frolova and I. T. S. Li, “Targeting Capabilities of Native and Bioengineered Extracellular Vesicles for Drug Delivery.,” *Bioengineering (Basel)*, vol. 9, no. 10, Sep. 2022, doi: 10.3390/bioengineering9100496.

[78] V. Tamasi, K. Németh, and M. Csala, “Role of Extracellular Vesicles in Liver Diseases,” *Life*, vol. 13, no. 5, p. 1117, Apr. 2023, doi: 10.3390/life13051117.

[79] G. Di Rocco, S. Baldari, and G. Toietta, “Towards Therapeutic Delivery of Extracellular Vesicles: Strategies for In Vivo Tracking and Biodistribution Analysis.,” *Stem Cells Int*, vol. 2016, p. 5029619, 2016, doi: 10.1155/2016/5029619.

[80] B. Li *et al.*, “Delivery of vascular endothelial growth factor (VEGFC) via engineered exosomes improves lymphedema,” *Ann Transl Med*, vol. 8, no. 22, pp. 1498–1498, Nov. 2020, doi: 10.21037/atm-20-6605.

Table of Abbreviations

ASCs	Adipose-Derived Stromal Cells
BCA	Bicinchoninic Acid Protein Assay
BECs	Blood Vascular Endothelial Cells
BSA	Bovine Serum Albumin
CMDR	Cellmask™ Deep Red
CRE	cAMP Response Element CRE
CREB	CRE Binding Protein
DMEM – HG	Dulbecco's Modified Eagle's Medium-High Glucose
Double	CD81-P1-VEGF-C/P1-VEGF-C
DPBS	Dulbecco’s Phosphate Buffered Saline
ECs	Endothelial Cells
eNOS	Endothelial Nitric Oxide Synthase
ER	Endoplasmic Reticulum
EVs	Extracellular Vesicles
F.I.	Fluorescence Intensity
FCS	Fetal Calf Serum
FIGF	c-Fos-Induced Growth Factor
HDLECs	Human Dermal Lymphatic Endothelial Cells
hTERT	Human Telomerase Reverse Transcriptase
LECs	Lymphatic Endothelial Cells
MAPK	Mitogen–Activated Protein Kinase
MMPs	Matrix Metalloproteinases
MSCs	Mesenchymal Stem Cell
mTOR	Mechanistic Target of Rapamycin
NRPs	Neuropilins
NTA	Nanoparticle Tracking Analysis
PI3K	Phosphoinositide 3-Kinase
PIGF	Placental Growth Factor
PLE	Primary Lymphoedema
RFU	Relative Fluorescence Units
Single	CD81-P1-VEGF-C
SLE	Secondary Lymphoedema
SN	Supernatant
TBST	Tris-Buffered Saline With Tween 20
TFF	Tangential Flow Filtration
UPR	Unfolded Protein Response
VEGF	Vascular Endothelial Growth Factor
VEGFR	VEGF Receptor
WR	Working Reagent

WT	Wild Type

List of figures

List of tables